FULL PAPER

ARCH PHARM
Archiv der Pharmazie
DPhG

Development of new pyrazoles as class I HDAC inhibitors: Synthesis, molecular modeling, and biological characterization in leukemia cells

Francesco Berluti[1] | Fady Baselious[1] | Sven Hagemann[2] |
Sebastian Hilscher[3] | Matthias Schmidt[1] | Stefan Hüttelmaier[2] |
Mike Schutkowski[3] | Wolfgang Sippl[1] | Hany S. Ibrahim[1,4]

[1]Department of Medicinal Chemistry, Institute of Pharmacy, Martin-Luther University Halle-Wittenberg, Halle (Saale), Germany

[2]Department of Molecular Medicine, Faculty of Medicine, Martin-Luther University Halle-Wittenberg, Halle (Saale), Germany

[3]Department of Enzymology, Institute of Biochemistry, Martin-Luther University Halle-Wittenberg, Halle (Saale), Germany

[4]Department of Pharmaceutical Chemistry, Faculty of Pharmacy, Egyptian Russian University, Badr City, Cairo, Egypt

Correspondence
Hany S. Ibrahim, Department of Medicinal Chemistry, Institute of Pharmacy, Martin-Luther University Halle-Wittenberg, 06120 Halle (Saale), Germany.
Email: hany.ibrahim@pharmazie.uni-halle.de

Funding information
Alexander von Humboldt-Stiftung; Deutsche Forschungsgemeinschaft; German Research Foundation DFG project,
Grant/Award Numbers: 495271833, 468534282; Alexander von Humboldt Foundation project EGY,
Grant/Award Number: 1191187

Abstract

Class I histone deacetylases (HDACs) are considered promising targets in current cancer research. To obtain subtype-selective and potent HDAC inhibitors, we used the aminobenzamide scaffold as the zinc-binding group and prepared new derivatives with a pyrazole ring as the linking group. The synthesized compounds were analyzed in vitro using an enzymatic assay against HDAC1, −2, and −3. Compounds **12b**, **15b**, and **15i** were found to be potent HDAC1 inhibitors, also in comparison to the reference compounds entinostat and tacedinaline, with IC_{50} values of 0.93, 0.22, and 0.68 µM, respectively. The best compounds were measured for their cellular effect and target engagement in acute myeloid leukemia (AML) cells. In addition, we studied the interaction of the compounds with HDAC subtypes using docking and molecular dynamic simulations. In summary, we have developed a new chemotype of HDAC1 inhibitors that can be used for further structure-based optimization.

KEYWORDS
aminobenzamide, class I HDAC, molecular docking, pyrazoles, tacedinaline

1 | INTRODUCTION

Histone modification is one of the most intensively studied epigenetic regulation. It involves the alteration of histone tails by various processes that regulate the balance between acetylation and deacetylation. This balance can be controlled by two reversible processes carried out by two families of enzymes: Histone acetyltransferases (HATs) and

histone deacetylases (HDACs).[1] HATs catalyze the attachment of acetyl groups to the ε-amino group of lysine residues of histones, resulting in loss of positive charge and decreased interactions between histone proteins and DNA.[2,3] Conversely, HDACs remove acetyl groups, which can lead to the formation of condensed chromatin (heterochromatin) and suppression of gene transcription. The dynamic control of histone acetylation by different classes of HDAC enzymes is

an important factor in shaping gene expression patterns and influencing cellular processes.[4,5] An imbalance in this regulation has been linked to the development of disease, with involvement in cancer being particularly emphasized. There are 18 different human HDAC subtypes, which are divided into four groups based on their phylogeny and domain organization: (i) class I (HDAC1, −2, −3, and −8), class IIa (HDAC4, −5, −7, and −9), class IIb (HDAC6 and −10), and class IV (HDAC11) which are zinc-dependent deacetylases, and (ii) class III (sirtuins) which are NAD$^+$-dependent enzymes.[6]

Class I HDACs (HDAC1, −2, −3, and −8) are the primary nuclear deacetylases responsible for regulating transcription through the modification of the lysine acetylation status on histone and nonhistone proteins (e.g., p53 in case of HDAC8). In contrast to the evolutionarily more distant HDAC8, the three closely related isoforms, HDAC1, HDAC2, and HDAC3, exhibit stable associations with other proteins and form well-defined nuclear co-repressor complexes.[7] They play a crucial role in cell proliferation, the progression of the cell cycle, and the establishment and maintenance of an abnormal phenotype observed in different types of cancers. Therefore, class I HDACs are considered validated targets for cancer treatment.[8]

HDAC inhibitors show a common pharmacophore consisting of a zinc-binding group (ZBG) followed by a linker and a capping group. The first HDAC inhibitors approved by the Food and Drug Administration (FDA) were characterized by the presence of a hydroxamate group as the ZBG, such as vorinostat, panobinostat, and belinostat.[9] HDAC inhibitors with a hydroxamate group as ZBG show disadvantages, such as poor bioavailability and stability as well as potential mutagenic potential.[10] Various functional groups, for example, aminobenzamides, which are characterized by good selectivity toward HDAC1, 2, and 3, have been developed as alternative ZBGs (Figure 1). Entinostat (I) and mocetinostat (II) are class I selective HDAC inhibitors and are in clinical trials for the treatment of various cancers either alone or in combination therapies.[11–14] We recently analyzed the effects of class I HDAC inhibitors (aminobenzamides) (HI2.1, 19f) (Figure 1) on different AML cancer cell lines and got promising results.[15,16] Therefore, we concentrated on the MV-4-11 cell line in this article. In addition, it is known that this cell line has a high expression of class I HDACs as reported.[17,18] To exclude HDAC3 from being targeted by aminobenzamide derivatives, an aromatic substituent should be added to this moiety to target the foot pocket of both HDAC1 and HDAC2, whereas this region is not accessible in HDAC3. This concept was confirmed by a crystallographic study in which a selective HDAC1 and HDAC2 inhibitor with a thienyl substituent was obtained (III, Figure 1).[19,20]

Tacedinaline (CI-994, IV) (Figure 2a) is a class I HDAC selective aminobenzamide-based inhibitor that has shown potent activity against various cancers such as AML,[21] prostate,[22] and lung cancer.[23] A recent study illustrated its activity against myelocytomatosis-driven medulloblastoma.[24] For this reason, we have taken tacedinaline and its thienyl derivative (V) as starting points for the synthesis of further class I HDAC inhibitors in the current study (Figure 2a). In a previous study, we designed a compound (HI12.1, 30c) and found that a simple extension of the tacedinaline scaffold can lead to a potent HDACi.[25] Therefore, we tested the insertion of a pyrazole ring between the phenyl and aminobenzamide moiety of tacedinaline, as shown in Figure 2 (12a–f and 15a–i) (Figure 2b). The preliminary docking study showed that it has the ability to interact with both aromatic residues F150 and H178 in the tunnel of HDAC active side (Figure 2b) (more details were discussed in the molecular modeling part). The pyrazole ring that was employed in the design allows us to use two different positions (position 4 and position 5) for the insertion of the aminobenzamide moiety, and that will provide more compounds with the same skeleton but they are different in the positional orientation of the aminobenzamide moiety. Furthermore, derivatives were prepared that additionally address both the HDAC1 and HDAC2 foot pockets. The third variation concerned the
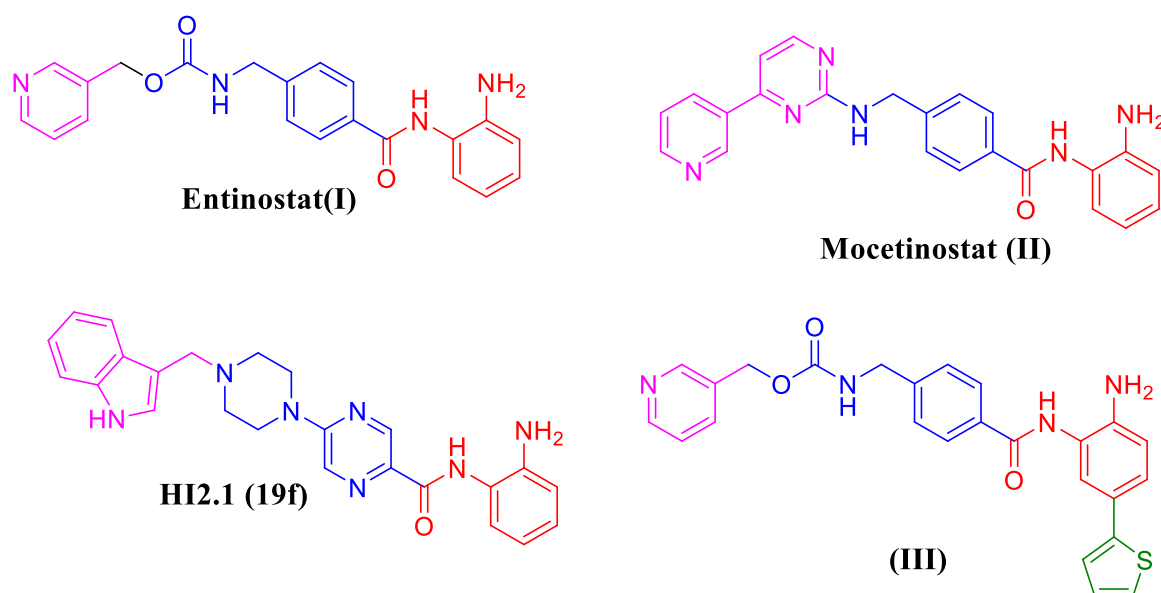
FIGURE 1 2-Aminobenzamide derivatives as class I histone deacetylase (HDAC) inhibitors. The skeleton of the inhibitors is colored according to their function inside the HDAC active site (ZBG: red, Foot pocket residue: green, linker: blue, capping group: pink).

(a)

Tacedinaline (IV)　　　　(V)　　　　HI12.1 (30c)

(b)　　The employment of pyrazole as a linker group
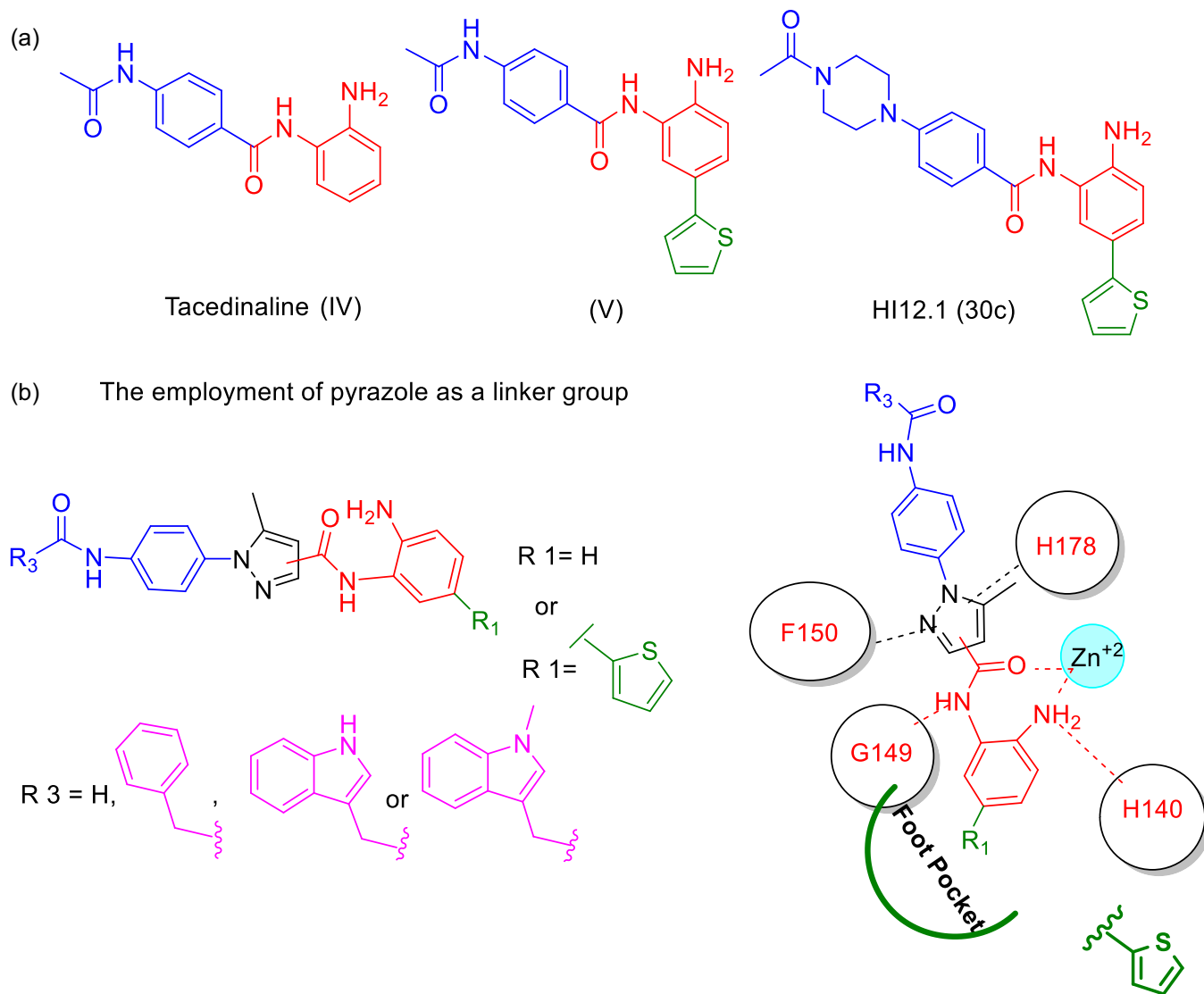
FIGURE 2 (a) 2-Aminobenzamide derivatives (Tacedinaline, **V** and HI12.1 (**30c**)) as lead compounds were used as starting points for the current work. (b) The proposed design strategy of the targeted compounds and the role of the pyrazole linker inside the binding pocket of histone deacetylase 1 (HDAC1).

attachment of different capping groups that can interact with the entry region of HDACs (Figure 2). The synthesized compounds were profiled in vitro for their HDAC activity and the best candidates were tested on AML cells for their antiproliferative effect.

## 2 | RESULTS AND DISCUSSION

2.1 | Chemistry

For the preparation of 5-methyl-1-(4-nitrophenyl)-1H-pyrazole-4-carboxylic acid (4) and its isomer 5-methyl-1-(4-nitrophenyl)-1H-pyrazole-3-carboxylic acid (8), the same methods were used as described by us in earlier work[26] (Schemes 1 and 2). The conversion of the two isomeric acid derivatives 4 and 8 to the aminobenzamide target compounds **12a–f** and **15a–i** was carried out in three

steps (Schemes 3 and 4). First, the coupling of acid derivatives 4 or 8 with mono-Boc-protected diamine derivatives (**9a–e**), which were prepared as reported,[15] using HATU (O-N,N,N′,N′-tetramethyluronium-hexafluorophosphate) in the presence of DIPEA (N,N-diisopropylethylamine) as a basic catalyst. Subsequently, the nitro group was reduced with Fe(acac)3 as an inorganic catalyst and hydrazine hydrate as a hydrogen source to obtain the amine derivatives **11a–d** and **14a–c**. Finally, to attach the capping group, we used the amide coupling with acid chloride derivatives and basic catalysts or the coupling with HATU and DIPEA as catalysts. This was followed by deprotection with trifluoroacetic acid (TFA) in dichloromethane (DCM) and neutralization with 1N NaOH to give the final compounds **12a–f** and **15a–i** (Scheme 3 and Table 1, Scheme 4 and Table 2).

Here, we have prepared a series of pairs that are isomeric due to the different substitutions on the pyrazole ring, such as **12a** and **15a** or **12f** and **15e**. The different substitution or isomerism results in a
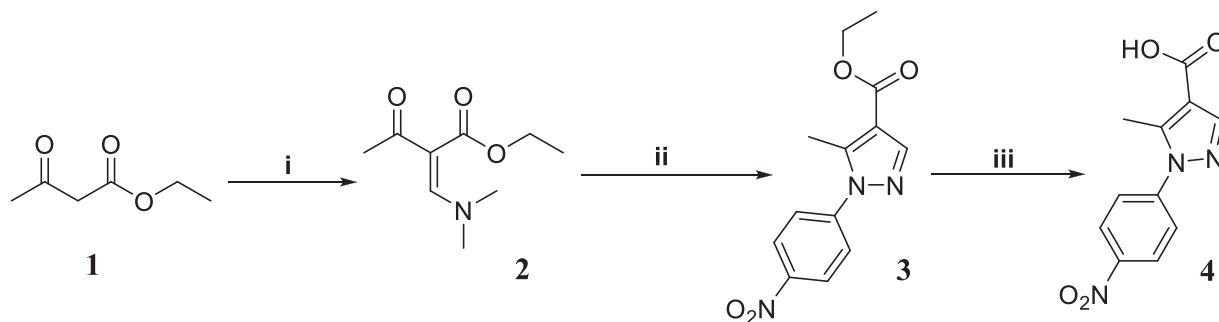
SCHEME 1 Synthesis of intermediate carboxylic acid **4**. Reagents and conditions: (i) DMF, DMA, reflux, 2 h. (ii) MeOH, reflux, 4 h, 70°C. (iii) MeOH, 1N NaOH, H_2O, reflux, 3 h, 70°C. DMF, dimethyl formamide.
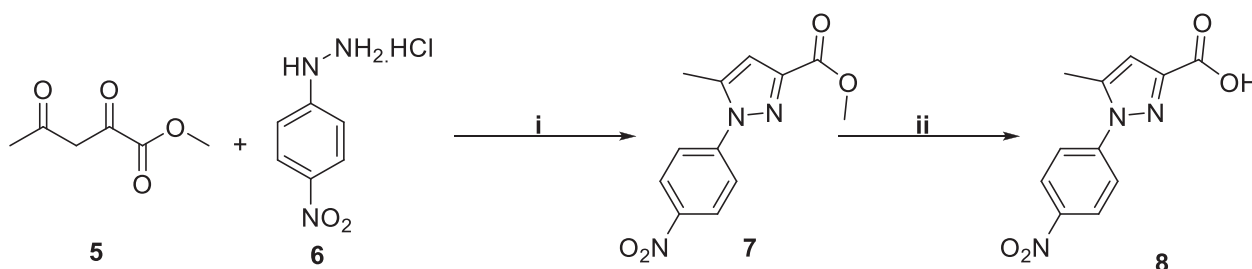

SCHEME 2 Synthesis of intermediate carboxylic acid **8**. Reagents and conditions: (i): CH_3COOH, H_2O, reflux,3 h. (ii): MeOH, 1N NaOH, H_2O, reflux, 3 h, 70°C.
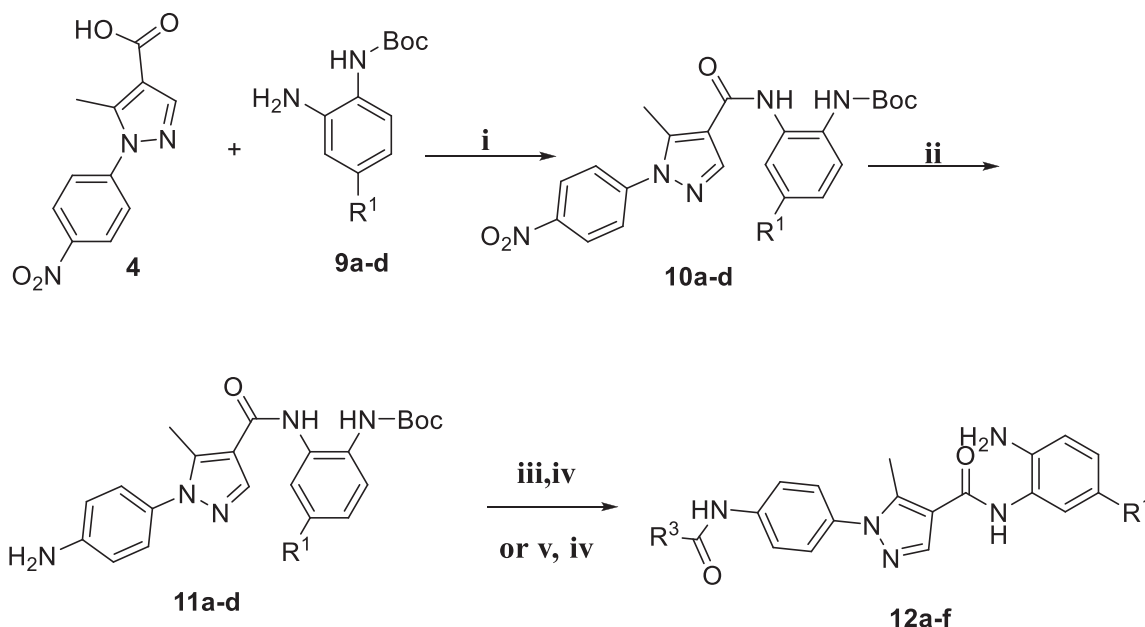
SCHEME 3 Synthesis of aminobenzamides (**12a–f**). Reagents and conditions: (i): HATU, DIPEA, DMF, overnight, 70°C. (ii): MeOH, NH_2NH_2-H_2O, Fe(acac)$_3$. (iii): RCOCl, TEA. DCM, 18 h, 0°C, then RT. (**12a–e**) (iv) DCM, TFA, 0°C,1 h, followed by 1N NaOH. (v) phenyl acetic acid or 2-(1-methyl-1H-indol-3-yl)acetic acid, HATU, DIPEA, DMF, 48 h, 70°C (**12f**). DIPEA, *N,N*-diisopropylethylamine; HATU, *O-N,N,N′,N′*-tetramethyluronium-hexafluorophosphate. DCM, dichloromethane; DMF, dimethyl formamide; TEA, triethyl amine; TFA, trifluoroacetic acid.

different spatial orientation of the capping group in the acetyl lysine tunnel of HDACs to possibly obtain a better subtype selectivity. The resulting isomer pairs can be clearly distinguished by the position of the proton of the pyrazole in the ^{1}HNMR analysis. H5 in compounds **12a–f** appears at 8.25 ppm for compounds with unsubstituted

aminobenzamide derivatives such as **12a**, **12e**, and **12f**. The substituted aminobenzamide derivatives with heteroaromatic rings such as 2-thienyl (**12b**), 2'-methoxyphenyl (**12c**), and 3'-methoxyphenyl (**12d**) showed a slight shift in H5 of pyrazole at 8.44, 8.55, and 8.47 ppm, respectively. On the other hand, H4 of pyrazole in compounds **15a–i**
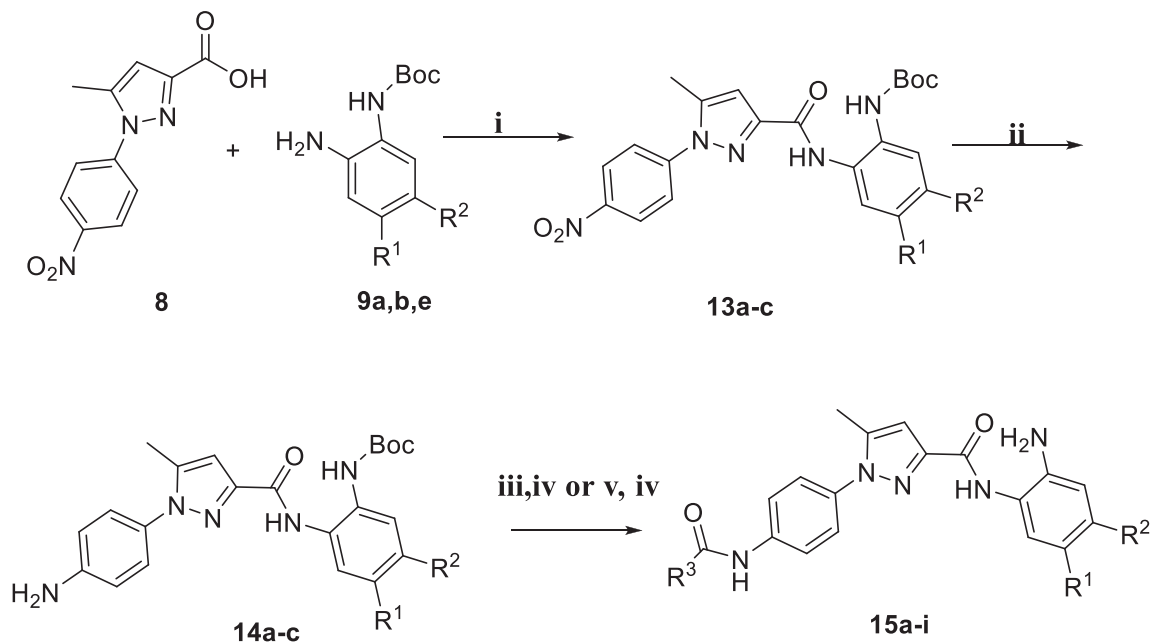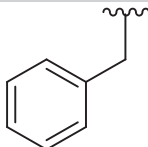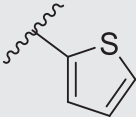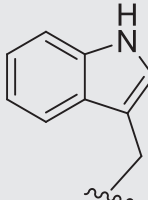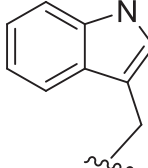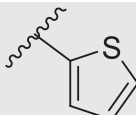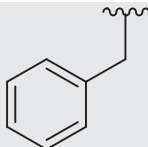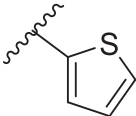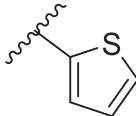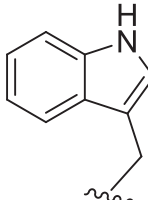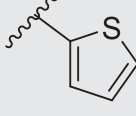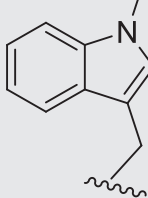
SCHEME 4 Synthesis of aminobenzamides (**15a–i**). Reagents and conditions: (i): HATU, DIPEA, DMF, overnight, 70°C. (ii): MeOH, NH_2NH_2–H_2O, Fe(acac)$_3$. (iii): RCOCl, TEA. DCM, 18 h, 0°C then RT. (**15a–d**, **15g**). (iv) DCM, TFA, 0°C,1 h, followed by 1N NaOH. (v) phenyl acetic acid, 2-(1H-indol-3-yl)acetic acid or 2-(1-methyl-1H-indol-3-yl)acetic acid, HATU, DIPEA, DMF, 48 h, 70°C (**15e,f,h,i**). DIPEA, N,N-diisopropylethylamine; HATU, O-N,N,N',N'-tetramethyluronium-hexafluorophosphate. DCM, dichloromethane; DMF, dimethyl formamide; TEA, triethyl amine; TFA, trifluoroacetic acid.

TABLE 1 Substituents of intermediates and final compounds as described in Scheme 3.

Comp. No.	R^1	R^3	Comp. No.	R^1	R^3
9a, 10a, 11a	H	----	**12b**		Me
9b, 10b, 11b		----	**12c**		Me
9c, 10c, 11c		----	**12d**		Me
9d, 11d, 11d		----	**12e**	H	
12a	H	Me	**12f**	H	

TABLE 2 Substituents of intermediates and final compounds in Scheme 4.

Comp. No.	R^1	R^2	R^3	Comp. No.	R^1	R^2	R^3
9a, 13a, 14a	H	H	----	15d	H	H	
9b, 13b, 14b		H	-----	15e	H	H	
9e, 13c, 14c	H	F	------	15f	H	H	
15a	H	H	Me	15g		H	
15b		H	Me	15h		H	
15c	H	F	Me	15i		H	

appeared in the range of 6.71–6.74 ppm with the exception of compounds **15a** and **15b** where the signals appeared at 6.81/6.822 ppm. Finally, all given compounds were purified by medium pressure liquid chromatography (MPLC) to obtain a purity of greater than 95% (confirmed by high-performance liquid chromatography [HPLC], see Methods section 4.1).

2.2 | Biological evaluation

2.2.1 | Enzymatic HDAC in vitro testing

All synthesized compounds were subjected to enzymatic inhibition test against HDAC1, −2, and −3 isoforms using Entinostat as reference compound as reported.[15] Class I HDAC member HDAC8 was not used for in vitro testing since aminobenzamides are known to be not active against HDAC8 as also reported in our previous work.[15] First, we tested compounds **12a,b** and **15a,b**. These compounds are characterized by the presence of an acetyl group as a small capping group with varying substituents on the aminobenzamide moiety. It was found that compounds **12b** and **15b** showed the best inhibitory activity against HDAC1 (IC$_{50}$ = 0.93 and 0.22 µM, respectively) and HDAC2 (IC$_{50}$ = 4.7 and 2.5 µM, respectively) (Table 3). The thiophene ring acts as a foot pocket group for HDAC1/2 and prevents these compounds from binding to HDAC3. On the other hand, compounds **12a**, **15a**, and **15c** did not show any inhibition. Further foot pocket substituents were utilized as in compounds **12c** and **12d** but also did not result in active inhibitors. We concluded that both isomeric scaffolds can be used to employ them for developing active HDAC1, −2, and −3 inhibitors (Table 3).

In the second phase of the development of HDAC1,2, and 3 inhibitors from these scaffolds, we proposed a rationale to variate the capping group on both isomeric scaffolds by retaining unsubstituted aminobenzamide moiety or just adding thiophene group as foot pocket filler. We tried two different capping groups on the H5 pyrazole scaffold as in compounds **12e** and **12f** but they did not show any inhibitory activity against any used isoform. The use of these capping groups on this scaffold with substituted aminobenzamide with thiophene was not chemically feasible; therefore, we shifted our work to the other scaffold (H4 pyrazole). Compound **15d–f** were synthesized with different capping groups (phenyl, 3-indolyl, 1-methyl-3-indolyl; respectively) but unfortunately, they did not possess any significant inhibitory activity. Upon using these different capping groups with a combination of 5-thienyl aminobenzamide moiety as in compounds **15g–i**, all of them possessed inhibitory activity and the best one among them was **15i** with $IC_{50} = 0.68\,\mu M$ against HDAC1 and $IC_{50} = 2.10\,\mu M$ against HDAC2.

To assess the selectivity against other isoforms, compounds **12b**, **15b**, and **15i** were screened against HDAC6 and HDAC8 and they showed no activity.

2.2.2 | Cellular testing

The most promising inhibitors were then tested in a cell viability assay via a tetrazolium salt-based assay on wild-type AML MV-4-11 cells at $10\,\mu M$ (Table 4). IC_{50} value was determined for all the synthesized compounds. The inhibitors **12b** and **15i** showed an effect in the low micromolar range ($IC_{50} = 3.2$ and $3.4\,\mu M$, respectively), whereas entinostat showed an IC_{50} value of $0.2\,\mu M$. Other compounds displayed either weak or no activity. To check the cellular target engagement, histone H3 hyperacetylation was measured for **12b** and **15i** in MV-4-11 cells (Figure 3 and Table 5). When tested at the concentration of the IC_{50} value inhibitors, **12b** and **15i** showed the strongest hyperacetylation of histone H3.

2.3 | Molecular modeling results

2.3.1 | Molecular docking

To study the interaction of the newly prepared compounds on the class I HDACs, we first analyzed the binding mode of the developed inhibitors using docking and molecular dynamic (MD) simulations. The docking poses of the two potent inhibitors **15b** and **15i** in the HDAC1 and HDAC2 crystal structures (HDAC1 PDB: 4BKX and HDAC2 PDB: 4LY1) showed a comparable binding mode with bidentate chelation of the zinc ion via the amino-NH_2 of the 2-aminobenzamide moiety and the carbonyl oxygen of the amide group (Figure 4). The distances between the zinc ion and the chelator atoms are between 2.26 and 2.55 Å, which are consistent with the distances observed in X-ray structures of aminobenzamides bound to HDACs. In addition, hydrogen bonding was observed between the

NH_2 of the 2-aminobenzamide and His140/145 and His141/146 (HDAC1/2). The NH and the carbonyl oxygen of the amide group formed hydrogen bonds with Gly149/154 and Tyr303/308 (HDAC1/2), respectively. The pyrazole ring is located between the conserved aromatic residues Phe150/155 and Phe205/210 in HDAC1/2 and forms π–π interactions with Phe150/155 and His178/183. The acetyl group of **15b** and the extended methyl indole capping group of **15i** are directed to loops 5 and 6. The methyl indole group of **15i** shows a stacking interaction with Tyr204/Tyr209. The thiophene moiety is embedded in the foot pocket of HDAC1 and HDAC2 and shows van der Waals interactions with Met30/35, Leu139/144, and Cys151/156 (HDAC1/2).

The binding mode of compounds **12b** and **12e** was also studied by docking. Both compounds showed comparable poses in HDAC1 with bidentate chelation of the catalytic zinc ion (Figure 5A,B). **12b** and **12e** also demonstrated hydrogen bond interactions similar to compounds **15b** and **15i**. The thiophene moiety of **12b** is occupying the foot pocket and forming hydrophobic interactions resembling those observed for compounds **15b** and **15i**. π–π interactions were observed between the phenyl ring attached to the pyrazole group and Phe205 for both inhibitors.

Comparing the docking poses of the ligands from the **12** and **15** series revealed that the different attachment points of the capping groups on the pyrazole linker resulted in a slight shift of the capping group position toward Phe150 in the **12** series (Figure 5C,D). This shift is more pronounced in **12e** since it consequently influenced the position of the terminal phenyl group to be directed more toward loop 5 compared with **15i**. Interestingly, this shift in the pose did not affect the inhibitory activity of the isomeric compounds in HDAC1. Despite the shift in the docking pose, **12e** and **12b** are still able to chelate the zinc ion in a bidentate fashion and form hydrogen bond interactions that are essential for the activity, which might rationalize the retained activity in HDAC1.

2.4 | MD simulations

The MD simulations of HDAC-inhibitor complexes showed that the complexes are stable during the simulation time of 50 ns, the root mean square deviation (RMSD) values of the protein backbone are stabilizing between 1 and 2 Å while the zinc ion is showing RMSD values of ~1 Å (Supporting Information S2: Figures S1 and S2). The RMSD value of **15b** in HDAC1 and −2 is stabilizing at 1–2 Å (Figure 6a, c), while higher RMSD values were observed for the larger inhibitor **15i** (around 5 Å) in HDAC1 and HDAC2 (Figure 6b,d). This observation was further investigated by examining the MD trajectories, which showed that the methyl-indole group of **15i** is flipping to the opposite direction toward loop 5 during the simulation (Supporting Information S2: Figures S24 and S25). While the fluctuation of the more flexible capping group can be expected as it is exposed to solvent, all other inhibitor-heavy atoms are stable with deviations below 2 Å (Figure 7). This observation indicates that the docking poses of **15i** in HDAC1 and HDAC2 are stable and the

TABLE 3 Class I HDAC enzymatic testing for the synthetic inhibitors 12a–f and 15a–i.
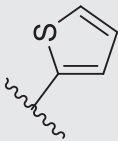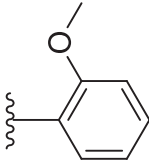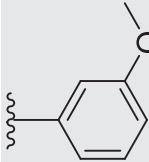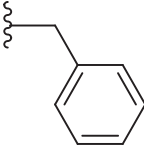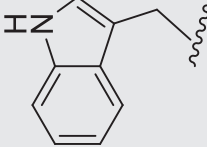
Comp. No.	R¹	R²	R³	HDAC1 IC$_{50}$ (µM)	HDAC2 IC$_{50}$ (µM)	HDAC3 IC$_{50}$ (µM)	HDAC 6	HDAC8
12a	H	-	Me	>20	>20	>20	ND	ND
12b	thiophen-2-yl	-	Me	0.93 ± 0.04	4.70 ± 0.2	>20	No Inhibition at 20 µM	19% Inhibition at 10 µM
12c	2-methoxyphenyl	-	Me	>20	>20	>20	ND	ND
12d	3-methoxyphenyl	-	Me	>20	>20	>20	ND	ND
12e	H	-	benzyl	1.19 ± 0.21	>20	>20	ND	ND
12f	H	-	(1H-indol-3-yl)ethyl	11.5 ± 1.1	>20	18.0 ± 2.8	ND	ND
15a	H	H	Me	>20	>20	>20	ND	ND

TABLE 3 (Continued)

Structures: **12a-f** and **15a-i**

Comp. No.	R^1	R^2	R^3	HDAC1 IC$_{50}$ (μM)	HDAC2 IC$_{50}$ (μM)	HDAC3 IC$_{50}$ (μM)	HDAC 6	HDAC8
15b	2-thienyl	H	Me	0.22 ± 0.02	2.5 ± 0.1	>20	No Inhibition at 20 μM	8% Inhibition at 10 μM
15c	H	F	Me	>20	>20	>20	ND	ND
15d	H	H	benzyl	>20	>20	>20	ND	ND
15e	H	H	(1H-indol-3-yl)ethyl	>20	17.9 ± 1.9	5.4 ± 0.4	ND	ND
15f	H	H	(1-methyl-1H-indol-3-yl)ethyl	>20	>20	6.5 ± 0.7	ND	ND
15g	2-thienyl	H	benzyl	1.42 ± 0.19	3.21 ± 1.25	>20	ND	ND
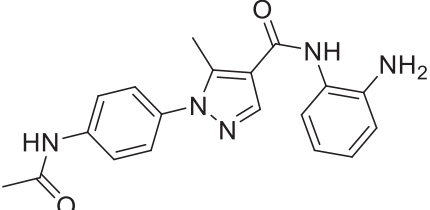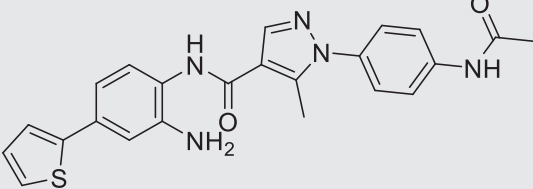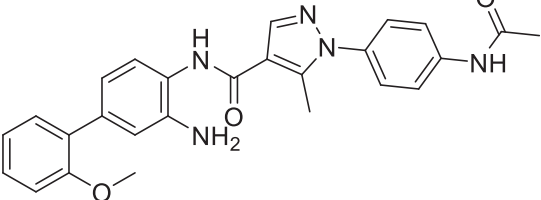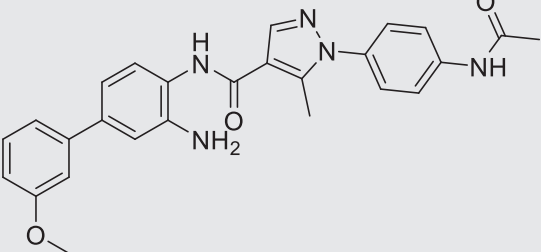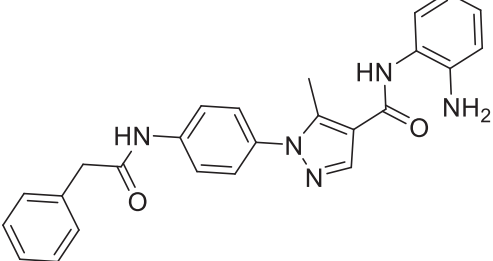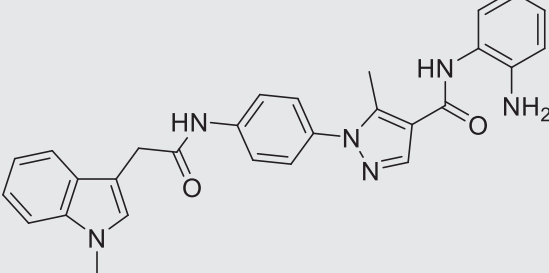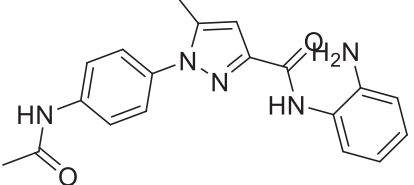
TABLE 3 (Continued)

Comp. No.	R¹	R²	R³	HDAC1 IC$_{50}$ (μM)	HDAC2 IC$_{50}$ (μM)	HDAC3 IC$_{50}$ (μM)	HDAC 6	HDAC8
15h	thiophene	H	indole (NH)	1.26 ± 0.26	4.41 ± 1.04	>20	ND	ND
15i	thiophene	H	N-methylindole	0.68 ± 0.15	2.10 ± 0.96	>20	No Inhibition at 20 μM	20% Inhibition at 10 μM
Tacedinaline	-	-	-	8.8 ± 1.2	7.5 ± 0.8	4.2 ± 0.5		
Entinostat	-	-	-	0.93 ± 0.1	0.95 ± 0.03	1.8 ± 0.1		

Abbreviation: ND; Not done.

TABLE 4 Cytotoxicity results of compounds 12b, 15d, and 15i against MV-4–11 cancer cells.

Comp. No.	Structure	IC$_{50}$ (μM)
12a		NA
12b		3.2 ± 0.9
12c		NA
12d		NA
12e		NA
12 f		14.6 ± 1.9
15a		NA

(Continues)

TABLE 4 (Continued)
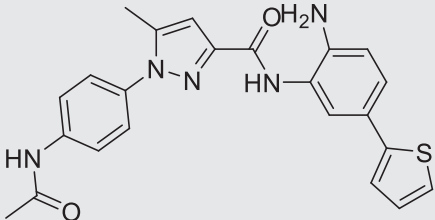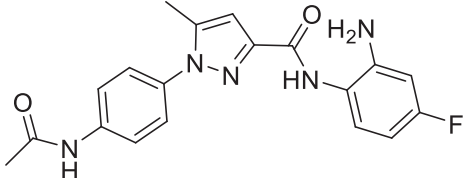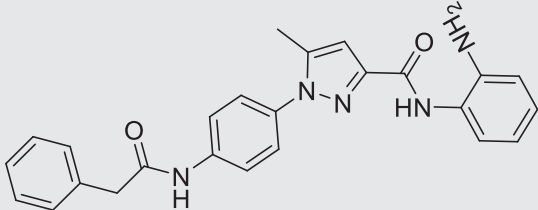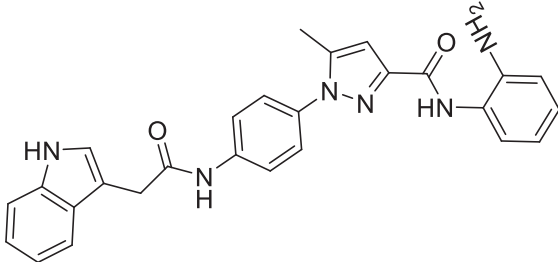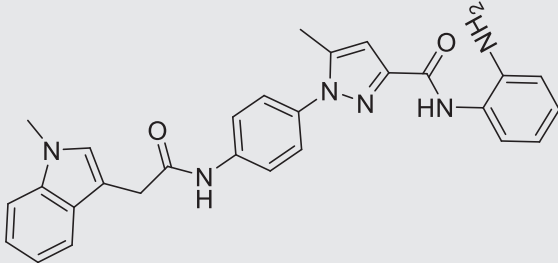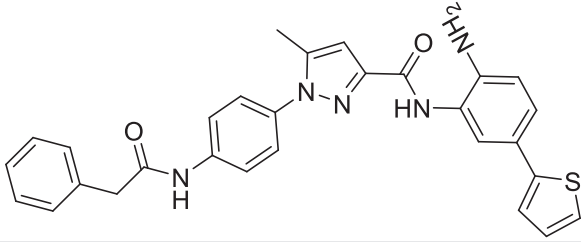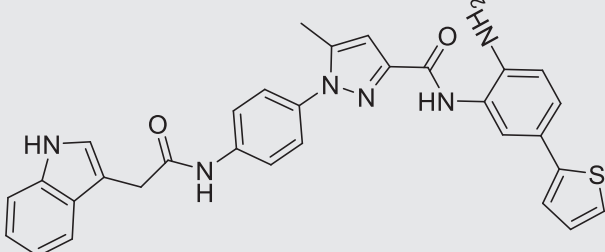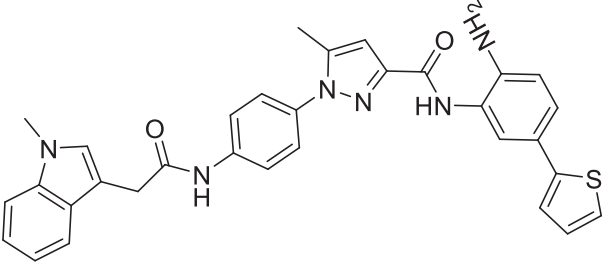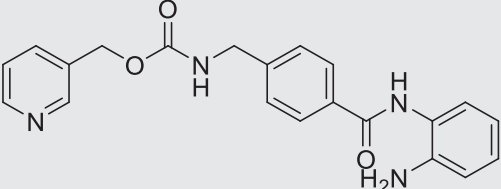
Comp. No.	Structure	IC$_{50}$ (µM)
15b		14.7 ± 1.5
15c		NA
15d		9.9 ± 0.6
15e		6.7 ± 0.2
15f		4.9 ± 0.6
15g		3.2 ± 0.3
15h		4.6 ± 0.1

TABLE 4 (Continued)

Comp. No.	Structure	IC$_{50}$ (µM)
15i		3.4 ± 0.8
Entinostat		0.2 ± 0.01

Abbreviation: NA, no activity.
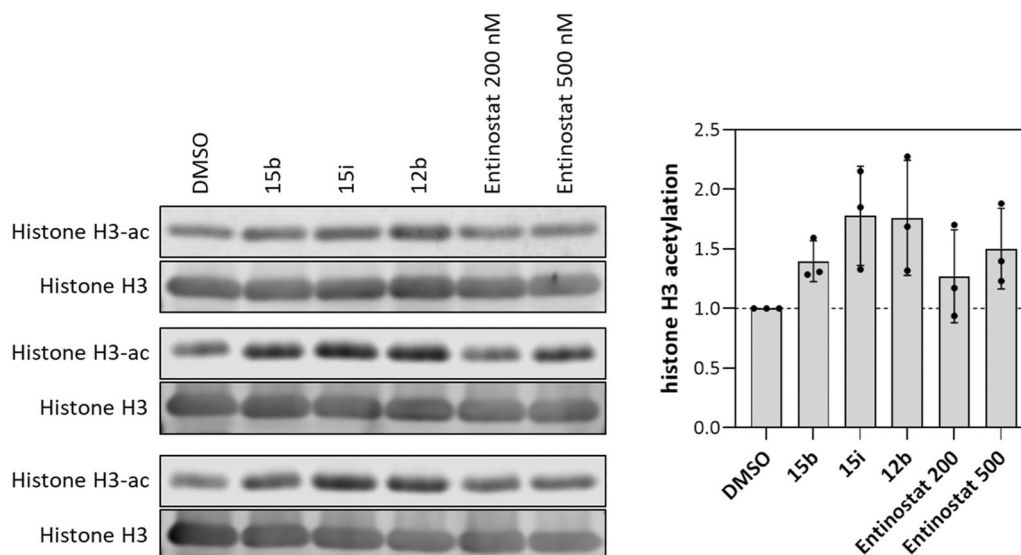
FIGURE 3 (a) Western blot assay to measure the effect of compounds **12b**, **15b**, and **15i** of the acetylation process of histone H3 acetylated histone H3 (triplicate). (b) Bar charts to show the quantification output of the acetylated histone during the Western blot assay (entinostat was used as reference).

TABLE 5 Relative histone H3 hyperacetylation of compounds 12b, 15b, and 15i during the western blot in MV-4-11 cancer cells (Entinostat was used as reference).

Comp. no.	Concentration	Relative histone H3 hyperacetylation	p Value
15i	10 µM	1.776 ± 0.34	0.0319
12b	5 µM	1.760 ± 0.39	0.0525
15b	20 µM	1.395 ± 0.14	0.0164
Entinostat	0.2 µM	1.269 ± 0.32	0.2983
Entinostat	0.5 µM	1.502 ± 0.28	0.0616

fluctuation of the capping group is responsible for the shift observed in the RMSD pattern of **15i**. This is also observed when inspecting the root mean square fluctuations (RMSF) plots which showed that the extended methyl-indole capping group is the most fluctuating part of the inhibitor with fluctuation of 2–3 Å in HDAC1 and 4–5 Å in HDAC2. In the case of **15b**, both in HDAC1 and HDAC2, RMSF values below 2 Å were detected (Figure 7, Supporting Information S2: Figures S24 and S25).

The hydrogen bonds for His140/145, His141/146, and Gly149/154 (HDAC1/2) showed high stability with persistence ranging between 77% and 100%, while for Tyr303/308 (HDAC1/2); the hydrogen bond was completely lost. The loss of hydrogen bond to
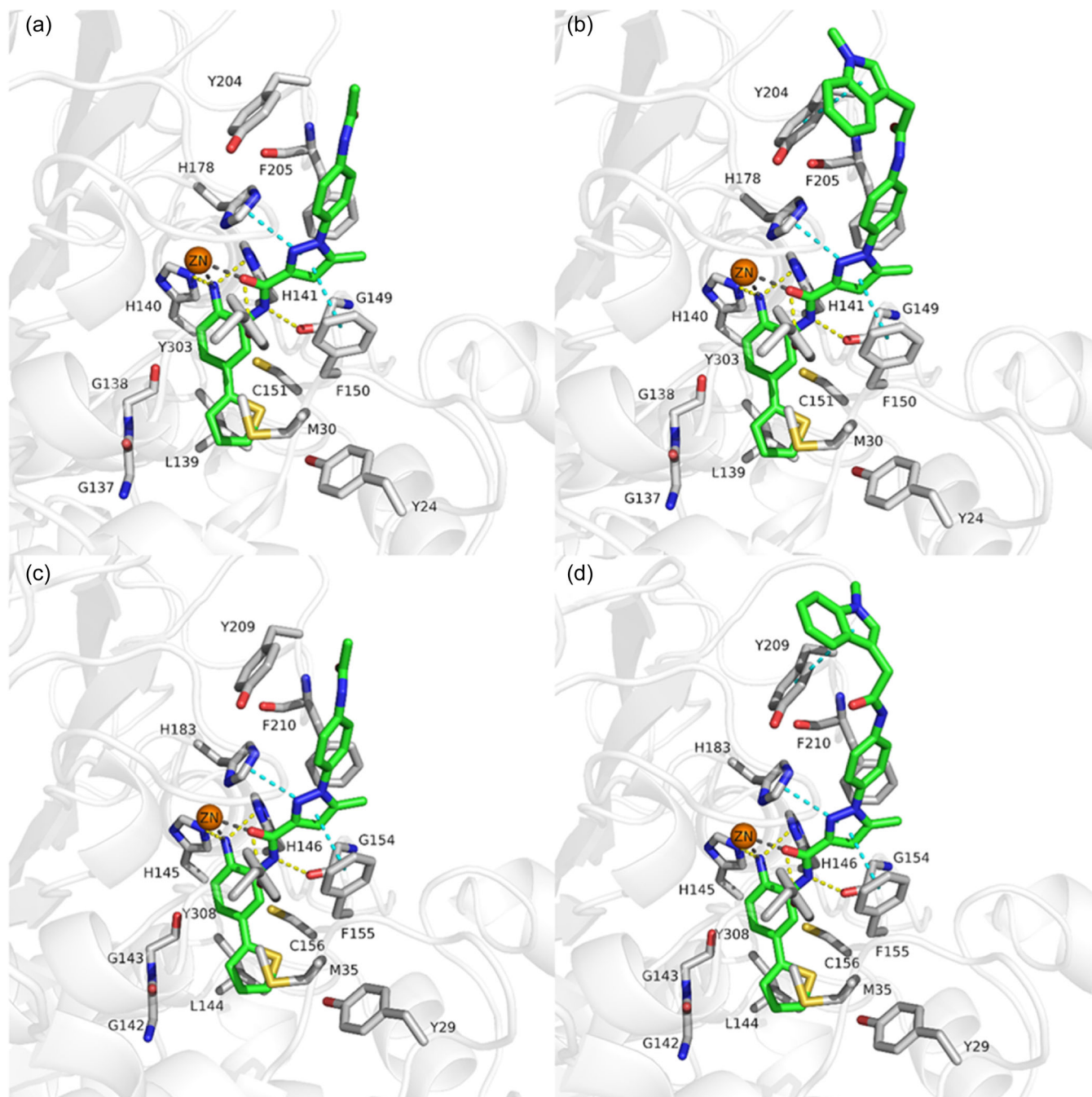
FIGURE 4 Docking poses of (a) **15b** in histone deacetylase 1 (HDAC1), (b) **15i** in HDAC1, (c) **15b** in HDAC2, and (d) **15i** in HDAC2. The protein backbone is shown as the white cartoon, the interacting residues are represented as gray sticks, the zinc ion as the orange sphere, and the inhibitors as green sticks. Coordination bonds are represented as gray dashed lines, hydrogen bonds as yellow dashed lines, and π –π interactions as cyan dashed lines.

Tyr303/308 (HDAC1/2) can be attributed to the flexibility of the side chain for this residue,[27,28] this behavior was also demonstrated in previous MD studies.[25,29] During the simulation, another hydrogen bond was formed between the carbonyl oxygen of the terminal amide and the backbone NH of Phe205/210 with persistence ranging between 61% and 94% (Supporting Information S2: Table S1 and Figures S9– S14).

The stability of bidentate chelation was monitored through the variation of the distances between the chelator atoms of the ligand and the zinc ion during the course of the simulation (Supporting Information S2: Figures S3 and S4). For both ligands in HDAC1 and HDAC2, the bidentate chelation mode observed initially in the docking poses was confirmed. Considering these results, it is worth noting that the flipping of the methyl indole moiety of **15i** did not affect the stability of key interactions of the ligand. Overall, the MD simulations verified the predicted binding mode of compounds **15b** and **15i** in HDAC1 and HDAC2 in terms of ligand RMSD, RMSF, and

FIGURE 5 (a, b) Docking poses of **12b** and **12e** in histone deacetylase 1 (HDAC1), respectively. The protein backbone is shown as the white cartoon, the interacting residues as gray sticks, the zinc ion as the orange sphere, and the inhibitors as green sticks. Coordination bonds are represented as gray dashed lines, hydrogen bonds as yellow dashed lines, and π –π interactions as cyan dashed lines. (c) Superposition of the docking poses of **12b** (red sticks) and **15b** (blue sticks) in HDAC1. (d) Superposition of the docking poses of **12e** (red sticks) and **15i** (blue sticks) in HDAC1. The zinc ion is represented as the orange sphere and the protein backbone as the white cartoon.

the stability of the bidentate chelation and the interactions that were observed initially.

The docking poses of compounds **12b** and **12e** in HDAC1 were also subjected to MD simulations. Both compounds demonstrated stable poses as indicated by ligand RMSD that is stabilizing at about 2 Å. However, few sharp fluctuations up to 4 Å are observed for **12e** (Figure 8a,b). Inspecting the RMSF plots as well as the MD

trajectories showed that the flexible capping group is responsible for these shifts (Figure 8c,d, Supporting Information S2: Figure S26).

The hydrogen bonds formed between the ligand and His140, His141, and Gly149 showed high stability with persistence ranging between 68% and 100% (Supporting Information S2: Table 1 and Figure S15–S17). Distances between the zinc ion and the chelator atoms of the ligands showed to be stable during the simulation
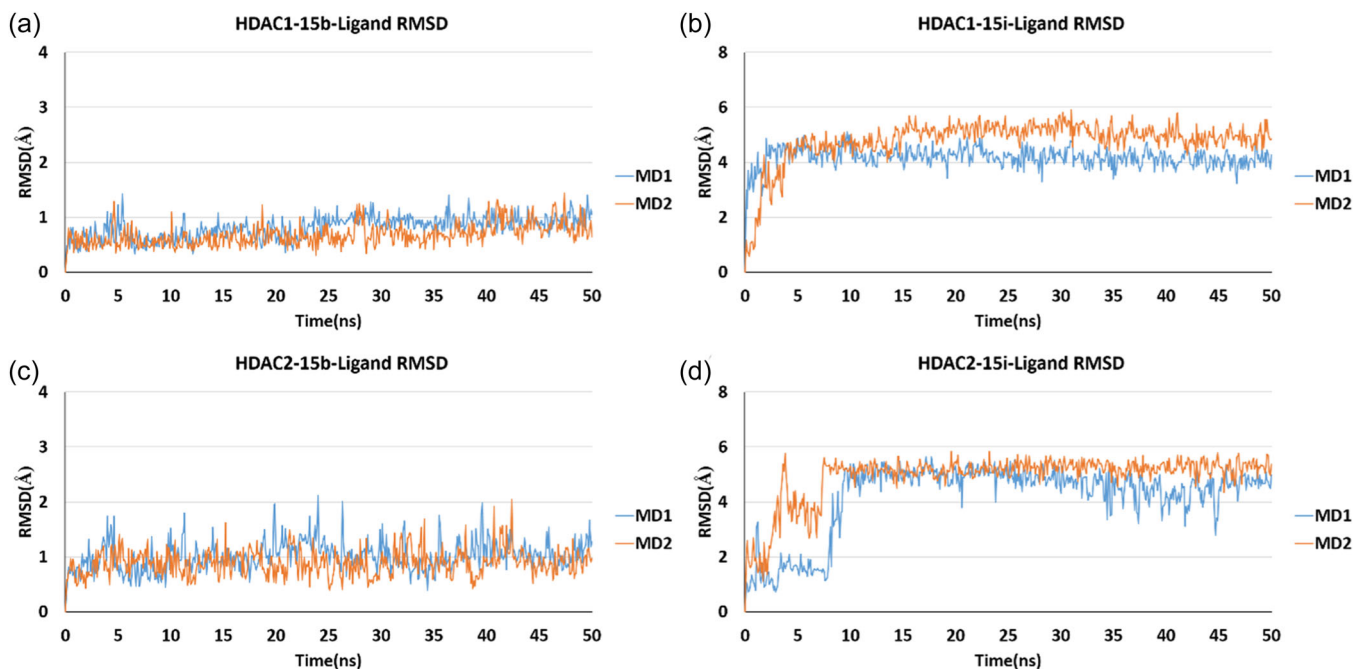
FIGURE 6 Root mean square deviation (RMSD) plots of the ligand for two independent molecular dynamic (MD) runs each for 50 ns. (a) **15b** in histone deacetylase 1 (HDAC1), (b) **15i** in HDAC1, (c) **15b** in HDAC2, (d) **15i** in HDAC2.
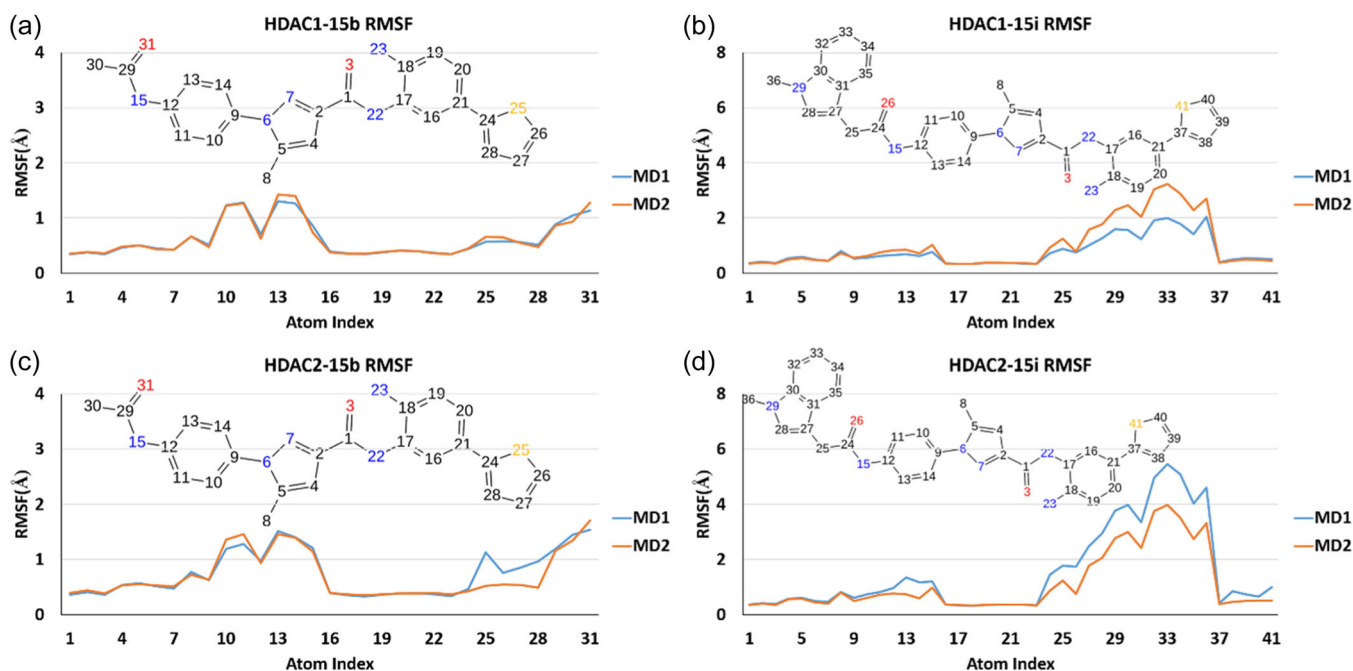
FIGURE 7 Root mean square fluctuations (RMSF) plots of ligands heavy atoms for two independent molecular dynamics (MD) runs each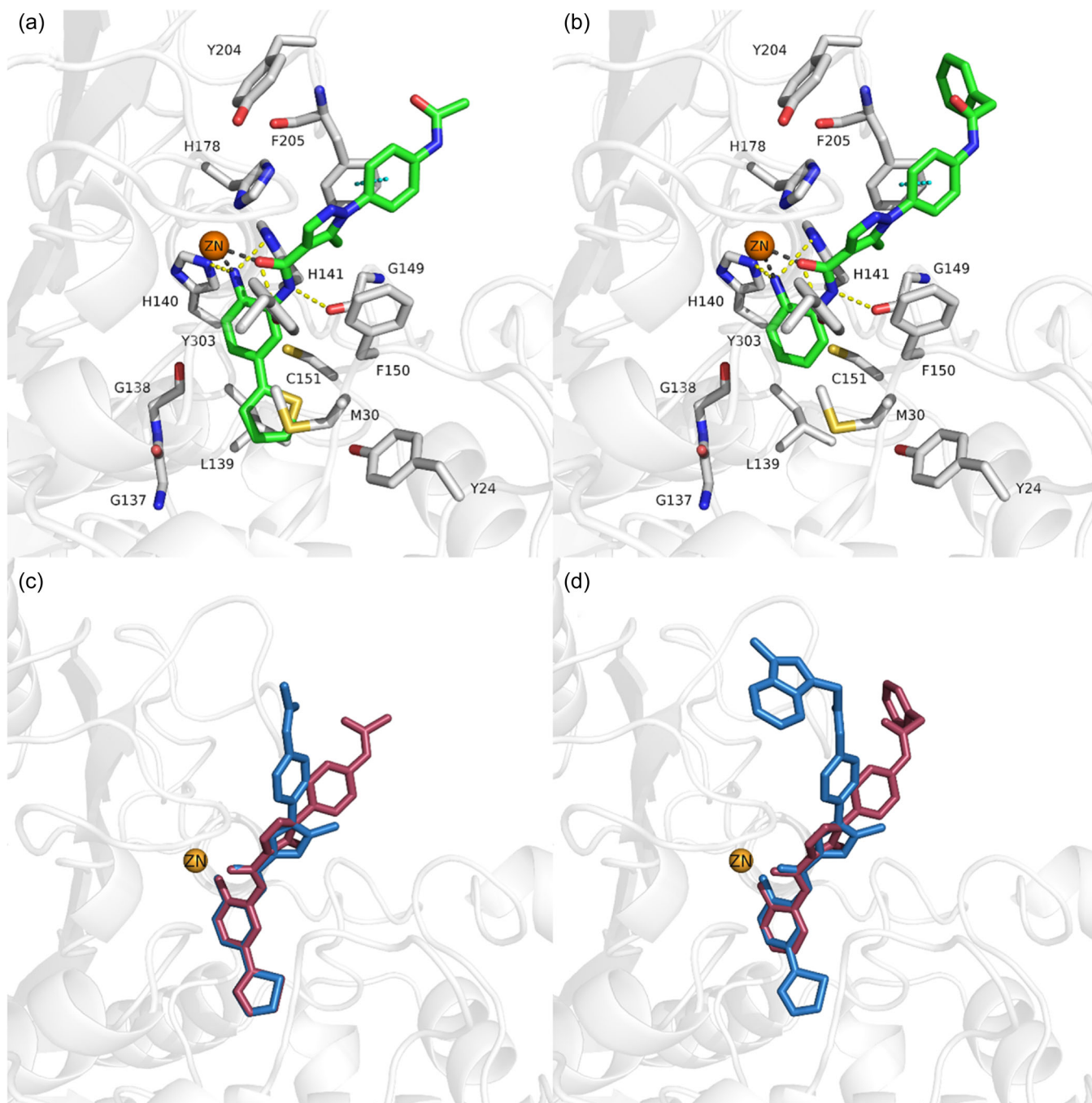 for 50 ns. (a) **15b** in histone deacetylase 1 (HDAC1), (b) **15i** in HDAC1, (c) **15b** in HDAC2, (d) **15i** in HDAC2.

course confirming the bidentate chelation mode of the ligands (Supporting Information S2: Figure S6).

To further challenge the stability of the protein–ligand complexes observed during the short MD simulations (50 ns), longer MD runs of 250 ns were executed. The analysis of the results confirmed the stability and showed similar behavior of the ligands compared with the shorter MD simulations. The RMSD plots of **12b** and **12e** in HDAC1 demonstrated that the ligands are stabilizing at around 2 Å, while the RMSD shifts up to 3–4 Å for **12e** are more pronounced (Figure 9a,b). Compound **15b** in HDAC1 and HDAC2 stabilized at an RMSD between 1 and 2 Å (Figure 9c,e), while for **15i**, the higher shifts due to the flipping of the extended methyl indole capping
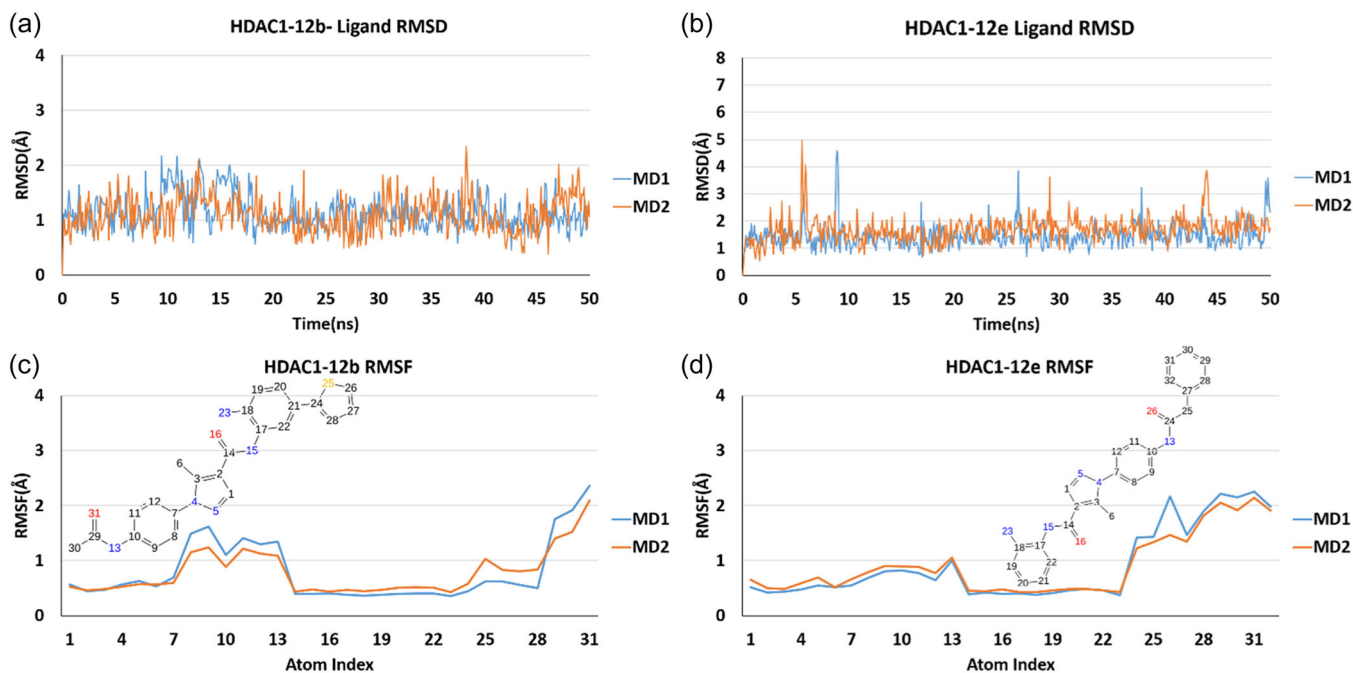
FIGURE 8   Root mean square deviation (RMSD) and root mean square fluctuations (RMSF) plots for two independent molecular dynamics (MD) runs each for 50 ns. (a, b) RMSD plots of ligand heavy atoms of **12b** and **12e**, respectively in histone deacetylase 1 (HDAC1). (c, d) RMSF plots of ligands heavy atoms of **12b** and **12e**, respectively in HDAC1.

group were also observed in the long MD simulations (Figure 9d,f, Supporting Information S2: Figures S7 and S27).

Inspecting the stability of the distance between the zinc ion and each of the amino-NH2 of the 2-aminobenzamide moiety and the carbonyl oxygen of the amide group confirmed the bidentate chelation initially observed in the docked poses for all the ligand–protein complexes (Supporting Information S2: Figures S8). The hydrogen bonds showed comparable stability to the shorter MD simulations in which the persistence of hydrogen bonds to His140/145, His141/146, and Gly149/154 (HDAC1/2) ranged between 74% and 99% and completely lost while for Tyr303/308 (HDAC1/2). For **15b** and **15i**, the additional hydrogen bonds formed during the simulation with Phe205/210 were also observed and showed persistence ranging between 45% and 93% (Supporting Information S2: Table 2 and Figure S18-S23).

3 | CONCLUSION

In the current study, we synthesized new selective HDAC class I inhibitors by inserting a pyrazole ring instead of the classical phenyl ring as a linking element between the ZBG (aminobenzamide) and the capping group. By using the two substituted pyrazole isomers, a different orientation of the capping group could be realized. Docking and MD simulations were used to check whether both pyrazole isomers fit into the HDAC1,2 binding pocket. A comparison of the in vitro HDAC activities of the isomers **12b** and **15b** showed that the more angled isomer **15b** exhibited greater selectivity HDAC1 to HDAC2, also in comparison to the reference entinostat. The introduction of an

additional capping group in **15b**, leading to **15i**, did not result in an increase in HDAC1/2 inhibition.

Although **15b** showed the strongest HDAC1 inhibition in vitro, the compounds **15i/12b** were more potent in inhibiting growth in cellular testing in MV-4-11 AML cells. However, the three pyrazoles tested showed weaker inhibition compared with the reference entinostat. The extent to which the attenuation is due to lower HDAC2 inhibition or poorer cell viability or pharmacokinetics needs to be clarified in further studies.

The docking studies performed with the isomeric pyrazole compounds showed a slightly different orientation of the phenyl ring bound to the pyrazole. Docking of **15i** showed that the capping group (indole) protrudes from the binding pocket into the solvent region and thus cannot contribute directly to binding. The lack of interaction could also be observed in the MD simulations of **15i** with HDAC1 and 2; the indole ring shows high fluctuation during the simulation. These data show that further capping groups for **12b/15b** need to be tested to obtain more potent inhibitors. We have laid the foundation for this work with the present biological and structural results.

4 | EXPERIMENTAL

4.1 | Chemistry

4.1.1 | General

All the specifications regarding the standard materials, equipment, and devices used in the experimental methods are included in the
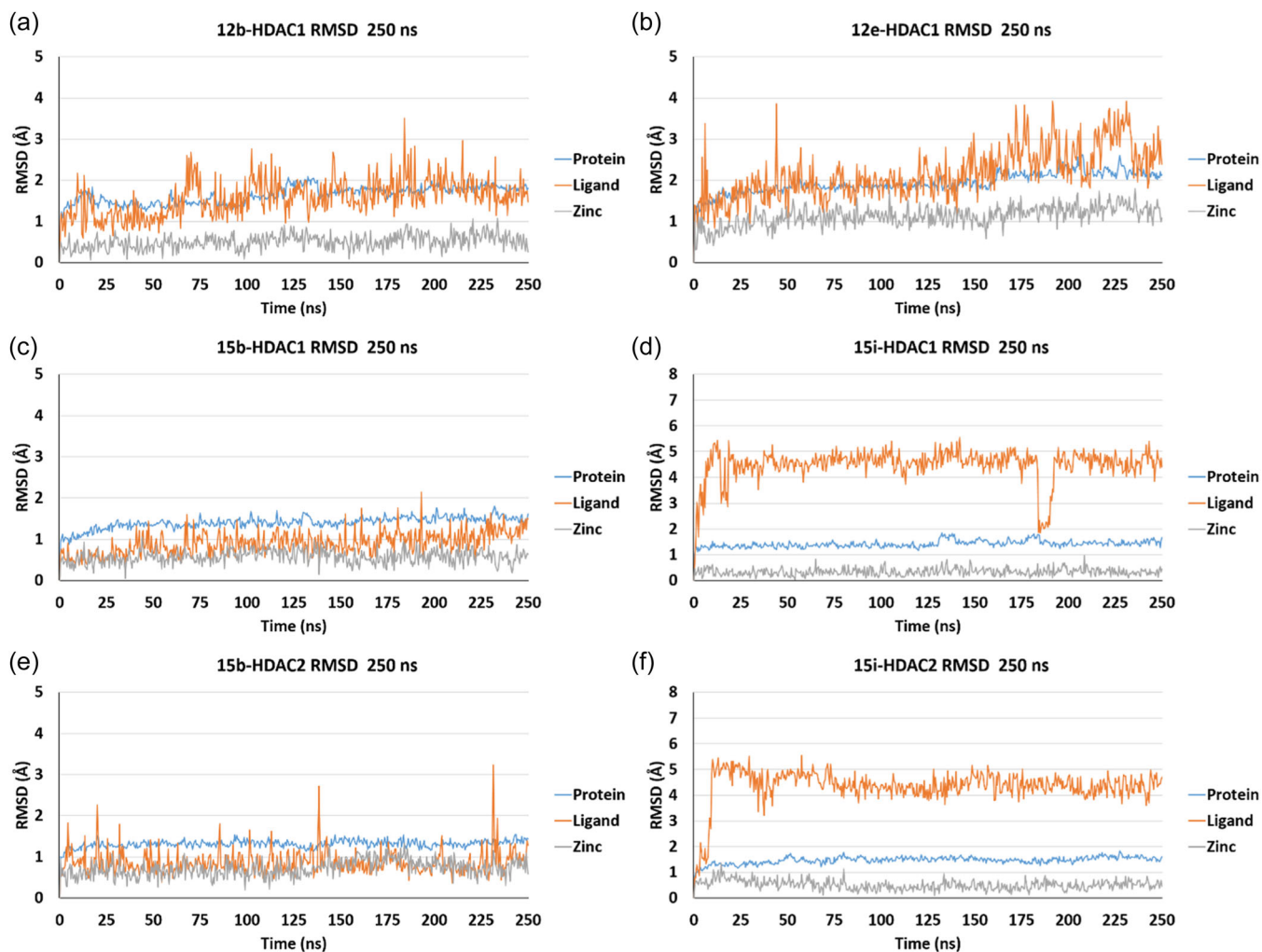
FIGURE 9 Root mean square deviation (RMSD) plots of protein backbone, ligands heavy atoms, and zinc ion for the long molecular dynamics (MD) runs (250 ns). (a) **12b** in histone deacetylase 1 (HDAC1), (b) **12e** in HDAC1, (c) **15b** in HDAC1, (d) **15i** in HDAC1, (e) **15b** in HDAC2, (f) **15i** in HDAC2.

Supporting Information. In addition, the experimental procedures for the synthesis of intermediates are included in Supporting Information. Compounds **9a** and **9b** were prepared as reported.[15]

The InChI codes of the investigated compounds, together with some biological activity data, are provided as Supporting Information.

4.1.2 | Synthesis of ethyl 5-methyl-1-(4-nitrophenyl)-1*H*-pyrazole-4-carboxylate (3)

A mixture of ethyl (Z)-2-((dimethylamino)methylene)-3-oxobutanoate (25) (1 eq.) and (4-nitrophenyl)hydrazine hydrochloride (10) (1 eq.) was dissolved in MeOH and it was stirred under reflux for 3 h. The mixture was cooled, and the solid formed was filtered under vacuum and concentrated under reduced pressure.[30] ^{1}H NMR (500 MHz, 400 MHz, DMSO-d^6) δ 8.37 (d, J = 9.2 Hz, 2H), 8.05 (s, 1H), 7.79 (d, J = 9.2 Hz, 2H), 4.33 (q, J = 6.4 Hz, 2H), 2.17 (s, 3H), 1.40 (t, J = 6.4 Hz, 3H). MS m/z: 276.091 [M + H], Yield 65%.

4.1.3 | Synthesis of methyl 5-methyl-1-(4-nitrophenyl)-1*H*-pyrazole-3-carboxylate (7)

A mixture of methyl 2,4-dioxopentanoate (5) (1eq.) and (4-nitrophenyl)hydrazine hydrochloride (6) (1eq.) was dissolved in a solution of acetic acid and water (4:1) and it was stirred under reflux for 3 h. The mixture was cooled, and the solid formed was filtered under vacuum and washed with hexane several times to eliminate the residues of acetic acid. ^{1}H NMR (400 MHz, DMSO-d^6) δ 8.38 (d, J = 9.2 Hz, 2H), 7.91 (d, J = 9.2 Hz, 2H), 6.84 (s, 1H), 3.82 (s, 3H), 2.44 (s, 3H). M S m/z: 262.075 [M + H]. Yield 75%.

4.1.4 | General procedure for ester hydrolysis to give carboxylic acid (4 and 8)

A mixture of the appropriate ester compound (**3 or 7**) was dissolved in H$_2$O (13 mL) and THF (13 mL). NaOH solution (1 g,17.82 mmol) in

H$_2$O (12 mL) was added and left stirring at room temprature (RT) for 2 h. Then, it was placed under an ice bath of HCl 1 M until it reached pH 5. The solid was filtered under a vacuum and it was washed with hexane to eliminate residual of HCl.

5-Methyl-1-(4-nitrophenyl)-1*H*-pyrazole-4-carboxylic acid (**4**)[30]: ^{1}H NMR (400 MHz, DMSO-*d*^{6}) δ 8.39 (d, *J* = 9.2 Hz, 2H), 8.11 (s, 1H), 7.88 (d, *J* = 9.2 Hz, 2H), 3.30 (s, 3H). MS *m/z*: 248.059 [M + H]. Yield 83%.

5-Methyl-1-(4-nitrophenyl)-1*H*-pyrazole-3-carboxylic acid (**8**): ^{1}H NMR (400 MHz DMSO-*d*^{6}) δ 8.37 (d, *J* = 9.2 Hz, 2H), 7.79 (d, *J* = 9.3 Hz, 2H), 6.50 (s, 1H), 2.33 (s, 3H). MS *m/z*: 248.059 [M + H]. Yield 85%.

4.1.5 | General procedure for nitro reduction (11a–d, 14a–c)

The nitro compound (1 g.) was diluted in acetonitrile (46 mL). Hydrazine monohydrate (2 mL) and a catalytic amount of iron(III) acetylacetone (0.1 g.) were added in reflux for 2 h. It is then filtered hot through celite, washed with methanol, and evaporated to obtain the compound in sufficient purity for the next step.

tert-Butyl *N*-{2-[1-(4-aminophenyl)-5-methyl-1*H*-pyrazole-4-amido] phenyl}carbamate (**11a**): ^{1}H NMR (400 MHz, DMSO-*d*^{6}) δ 9.47 (s, 1H), 8.54 (s, 1H), 8.40 (d, *J* = 9.1 Hz, 1H), 8.32 (s, 1H), 7.89 (d, *J* = 9.2 Hz, 1H), 7.54 (dd, *J* = 7.9, 1.7 Hz, 1H), 7.47 (dd, *J* = 7.8, 1.9 Hz, 1H), 7.12 (d, *J* = 8.8 Hz, 2H), 6.68 (d, *J* = 8.8 Hz, 2H), 4.01 (s, 2H), 2.43 (s, 3H), 1.44 (s, 9H). MS *m/z*: 408.3 [M + H]. Yield 64%.

tert-Butyl *N*-{2-[1-(4-aminophenyl)-5-methyl-1*H*-pyrazole-4-amido]-4-(thiophen-2-yl)phenyl}carbamate (**11b**): ^{1}H NMR (400 MHz, DMSO-*d*^{6}) δ 9.55 (s, 1H), 8.61 (s, 1H), 8.13 (s, 1H), 7.75 (d, *J* = 2.2 Hz, 1H), 7.61 (d, *J* = 8.6 Hz, 1H), 7.55–7.40 (m, 3H), 7.15–7.05 (m, 3H), 6.65 (d, *J* = 8.7 Hz, 2H), 5.14 (s, 2H) 2.07 (s, 3H), 1.45 (s, 9H). TLC: EtOAc/heptane (1:1) MS *m/z*: 390.1 [M + H]$^+$, 388.1 [M-H]$^-$. Yield 71%.

tert-Butyl *N*-{3-[1-(4-aminophenyl)-5-methyl-1*H*-pyrazole-4-amido]-2'-methoxy-[1,1'-biphenyl]-4-yl}carbamate (**11c**): ^{1}H NMR (400 MHz, DMSO-*d*^{6}) δ 9.50 (s, 1H), 8.61 (s, 1H), 8.11 (s, 1H), 7.62–7.52 (m, 2H), 7.34 (d, *J* = 1.8 Hz, 1H), 7.33–7.24 (m, 3H), 7.09 (d, *J* = 8.7 Hz, 2H), 7.02 (t, *J* = 7.5 Hz, 1H), 6.64 (d, *J* = 8.7 Hz, 2H), 5.42 (s, 2H), 3.76 (s, 3H), 2.42 (s, 3H), 1.46 (s, 9H). TLC: EtOAc/heptane (1:1) MS *m/z*:414.1, 514.1 [M + H]$^+$. Yield 78%.

tert-Butyl *N*-{3-[1-(4-aminophenyl)-5-methyl-1*H*-pyrazole-4-amido]-3'-methoxy-[1,1'-biphenyl]-4-yl}carbamate (**11d**): ^{1}H NMR (400 MHz, DMSO-*d*^{6}) δ 9.56 (s, 1H), 8.62 (s, 1H), 8.13 (s, 1H), 7.77 (d, *J* = 2.2 Hz, 1H), 7.64 (d, *J* = 8.5 Hz, 1H), 7.49 (dd, *J* = 8.5, 2.2 Hz, 1H), 7.36 (t, *J* = 8.0 Hz, 1H), 7.23–7.06 (m, 4H), 6.91 (ddd, *J* = 8.2, 2.6, 0.9 Hz, 1H), 6.65 (d, *J* = 8.7 Hz, 2H), 5.40 (s, 2H), 3.81 (s, 3H), 2.43 (s, 3H), 1.46 (s, 9H). TLC: EtOAc/heptane (1:1) MS *m/z*:414.1. Yield 72%.

tert-Butyl *N*-{2-[1-(4-aminophenyl)-5-methyl-1*H*-pyrazole-3-amido]-4-(thiophen-2-yl)phenyl}carbamate (**14b**): ^{1}H NMR (400 MHz, DMSO-*d*^{6}) δ 9.63 (s, 1H), 8.96 (s, 1H), 7.52 (d, *J* = 6.2 Hz, 1H), 7.46–7.39 (m, 2H), 7.32 (d, *J* = 8.4 Hz, 1H), 7.18–7.09 (m, 4H), 6.69 (s, 1H), 6.64 (d, *J* = 8.7 Hz, 2H), 5.44 (s, 2H), 2.24 (s, 3H), 1.37 (s, 9H). M S *m/z*: 490.2 [M + H]. Yield 66%.

tert-butyl *N*-{2-[1-(4-aminophenyl)-5-methyl-1*H*-pyrazole-3-amido]-5-fluorophenyl}carbamate (**14c**): ^{1}H NMR (400 MHz, DMSO-*d*^{6}) δ 9.58 (s, 1H), 8.95 (s, 1H), 7.66 (dd, *J* = 9.0, 6.2 Hz, 1H), 7.23 (dd, *J* = 10.5, 2.9 Hz, 1H), 7.13 (d, *J* = 8.7 Hz, 2H), 7.05–6.95 (m, 1H), 6.67 (s, 1H), 6.64 (d, *J* = 8.7 Hz, 2H), 5.43 (s, 2H), 2.22 (s, 3H), 1.38 (s, 9H). M S *m/z*: 426.2 [M + H]. Yield 75%.

4.1.6 | General procedure for amide coupling (10a–d, 13a–c)

A mixture of the appropriate carboxylic acid (1.0 eq.) and HATU (1.2 eq.) and the corresponding amine (1.1 eq.) were dissolved in dry dimethyl formamide (DMF) (25 mL) and DIPEA (4.0 eq.) was added. The reaction mixture was stirred at 70°C overnight. Brine (20 mL) was added to quench the reaction and then the aqueous solution was extracted with EtOAc (2 × 20 mL). The organic extract was washed with 2 N NH$_4$Cl, 1 N NaHCO$_3$, dried over anhydrous Na$_2$SO$_4$, filtered, and concentrated under reduced pressure. The residue was purified using MPLC (Heptane: EtOAc) (25%–35%).

tert-Butyl *N*-{2-[5-methyl-1-(4-nitrophenyl)-1*H*-pyrazole-4-amido] phenyl}carbamate (**10a**): ^{1}H NMR (400 MHz, DMSO-*d*^{6}) δ 9.60 (s, 1H), 8.54 (s, 1H), 8.40 (d, *J* = 9.0 Hz, 2H), 8.31 (s, 1H), 7.89 (d, *J* = 9.0 Hz, 2H), 7.56 (d, *J* = 9.1 Hz, 1H), 7.47 (d, *J* = 7.9 Hz, 1H), 7.18 (t, *J* = 8.5 Hz, 1H), 7.12 (t, *J* = 7.6 Hz, 1H), 2.64 (s, 3H), 1.44 (s, 9H). TLC: EtOAc/heptane (3:1) M S *m/z*: 438.3 [M + H]$^+$. Yield 41%.

tert-Butyl *N*-{2-[5-methyl-1-(4-nitrophenyl)-1*H*-pyrazole-4-amido]-4-(thiophen-2-yl)phenyl}carbamate (**10b**): ^{1}H NMR (500 MHz, DMSO-*d*^{6}) δ 9.69 (s, 1H), 8.62 (s, 1H), 8.40–8.35 (m, 3H), 7.90 (d, *J* = 9.0 Hz, 2H), 7.75 (d, *J* = 2.2 Hz, 1H), 7.64 (d, *J* = 8.5 Hz, 1H), 7.56–7.46 (m, 2H), 7.44 (dd, *J* = 3.6, 1.2 Hz, 1H), 7.12 (dd, *J* = 5.1, 3.6 Hz, 1H), 2.65 (s, 3H), 1.46 (s, 9H). TLC: EtOAc/heptane (3:1), MS *m/z*: 420.3, 520.3 [M + H]$^+$, 518.7 [M-H]$^-$. Yield 45%.

tert-Butyl *N*-{2'-methoxy-3-[5-methyl-1-(4-nitrophenyl)-1*H*-pyrazole-4-amido]-[1,1'-biphenyl]-4-yl}carbamate (**10c**): ^{1}H NMR (400 MHz, DMSO-*d*^{6}) δ 9.64 (s, 1H), 8.61 (s, 1H), 8.40 (d, *J* = 9.1 Hz, 2H), 8.32 (s, 1H), 7.89 (d, *J* = 9.0 Hz, 2H), 7.61–7.55 (m, 2H), 7.37–7.23 (m, 3H), 7.10 (dd, *J* = 8.4, 1.1 Hz, 1H), 7.02 (td, *J* = 7.5, 1.1 Hz, 1H), 3.76 (s, 3H), 2.64 (s, 3H), 1.46 (s, 9H). TLC: EtOAc/heptane (3:1) MS *m/z*: 444.1, 544.1 [M + H]$^+$. Yield 52%.

tert-Butyl *N*-{3'-methoxy-3-[5-methyl-1-(4-nitrophenyl)-1*H*-pyrazole-4-amido]-[1,1'-biphenyl]-4-yl}carbamate (**10d**): ^{1}H NMR (400 MHz, CDCl$_3$) δ 9.12 (s, 1H), 8.39 (d, *J* = 9.0 Hz, 2H), 8.10 (s, 1H), 8.04 (s, 1H), 7.70 (d, *J* = 9.0 Hz, 2H), 7.43–7.27 (m, 2H), 7.21–7.09 (m, 3H), 7.09 (d, *J* = 8.4, 1H), 6.78 (s, 1H) 3.85 (s, 3H), 2.75 (s, 3H), 1.53 (s, 9H). TLC: EtOAc/heptane (3:1) MS *m/z*: 444.1, 544.1 [M + H]$^+$, 542.3 [M-H]$^-$. Yield 37%.

tert-Butyl *N*-{2-[5-methyl-1-(4-nitrophenyl)-1*H*-pyrazole-3-amido] phenyl}carbamate (**13a**): ^{1}H NMR (400 MHz, DMSO-*d*^{6}) δ 9.60 (s, 1H), 8.54 (s, 1H), 8.40 (d, *J* = 9.0 Hz, 2H), 8.31 (s, 1H), 7.89 (d, *J* = 9.0 Hz, 2H), 7.56 (d, *J* = 9.1 Hz, 1H), 7.47 (d, *J* = 7.9 Hz, 1H), 7.18 (t, *J* = 8.5 Hz, 1H), 7.12 (t, *J* = 7.6 Hz, 1H), 2.64 (s, 3H), 1.44 (s, 9H). TLC: 1:1 (EtOAc/ heptane). MS *m/z*: 438.3 [M + H]. Yield 55%.

tert-Butyl *N*-{2-[5-methyl-1-(4-nitrophenyl)-1*H*-pyrazole-3-amido]-4-(thiophen-2-yl)phenyl}carbamate (**13b**): ^{1}H NMR (400 MHz, DMSO-*d*^{6}) δ 9.63 (s, 1H), 8.96 (s, 1H), 7.52 (d, *J* = 6.2 Hz, 1H), 7.46–7.39 (m, 2H), 7.32 (d, *J* = 8.4 Hz, 1H), 7.18–7.09 (m, 4H), 6.69 (s, 1H), 6.64 (d, *J* = 8.7 Hz, 2H), 2.24 (s, 3H), 1.37 (s, 9H). TLC: 1:1 (EtOAc/heptane). MS *m/z*: 518.2 [M−H]. Yield 45%.

tert-Butyl *N*-{5-fluoro-2-[5-methyl-1-(4-nitrophenyl)-1*H*-pyrazole-3-amido]phenyl}carbamate (**13c**): ^{1}H NMR (400 MHz, DMSO-*d*^{6}) δ 9.74 (s, 1H), 8.98 (s, 1H), 8.40 (d, *J* = 9.2 Hz, 2H), 7.94 (d, *J* = 9.2 Hz, 2H), 7.63 (dd, *J* = 9.0, 6.1 Hz, 1H), 7.27 (dd, *J* = 10.5, 3.0 Hz, 1H), 7.01 (td, *J* = 8.5, 3.0 Hz, 1H), 6.84 (s, 1H), 2.45 (s, 3H), 1.37 (s, 9H). TLC: 1:1 (EtOAc/heptane). MS *m/z*: 455.160 [M + H]. Yield 51%.

4.1.7 | General procedure for the synthesis of the final compounds 12f, 15e,15f, 15h, and 15i

A mixture of the appropriate carboxylic acid (1.0 eq.) and HATU (1.2 eq.) and the corresponding amine (1.1 eq.) were dissolved in dry DMF (25 mL) and DIPEA (4.0 eq.) was added; the reaction mixture was stirred at 70°C for 48 h. Brine (20 mL) was added to quench the reaction and then the aqueous solution was extracted with EtOAc (20 mL). The organic extract was washed with 2 N NH$_4$Cl, 1 N NaHCO$_3$, dried over anhydrous Na$_2$SO$_4$, filtered, and concentrated under reduced pressure. The residue was purified using MPLC (heptane/EtOAc) (35%). The solids were dissolved in DCM (5 mL), and then TFA (5 mL) was added at 0°C. The reaction mixture was stirred at RT for 1 h. The solvent was evaporated to dryness, and 1 N NaOH (20 ml) was added to the residue and the mixture was stirred for 1 h, then it was extracted with EtOAc. The organic extract was washed with brine, dried over anhydrous Na2SO4, filtered, and concentrated under reduced pressure. The residue was purified by using MPLC (heptane/EtOAc) (50%–60%).

N-(2-Aminophenyl)-5-methyl-1-{4-[2-(1-methyl-1*H*-indol-3-yl)acetamido]phenyl}-1*H*-pyrazole-4-carboxamide (**12f**): ^{1}H NMR (400 MHz, DMSO-*d*^{6}) δ 10.34 (s, 1H), 9.28 (s, 1H), 8.25 (s, 1H), 7.77 (d, *J* = 9.0 Hz, 2H), 7.65 – 7.58 (m, 1H), 7.43 (d, *J* = 9.0 Hz, 2H), 7.39 (d, *J* = 8.2 Hz, 1H), 7.25 (s, 1H), 7.16–7.10 (m, 2H), 7.04–6.99 (m, 1H), 6.96–6.91 (m, 1H), 6.76 (d, *J* = 8.0 Hz, 1H), 6.62–6.53 (m, 1H), 4.85 (s, 2H), 3.75 (s, 5H), 2.3 (s, 3H). ^{13}C NMR (101 MHz, DMSO-*d*^{6}) δ 170.34, 143.60, 142.39, 139.76, 137.00, 134.04, 128.67, 127.97, 127.15, 126.22, 123.69, 121.60, 119.78, 119.30, 118.99, 116.68, 116.52, 115.78, 110.04, 108.11, 34.07, 32.74, 11.95. TLC: 3:1 (EtOAc/heptane). HPLC: rt 12.18 min (purity 96.8%), MS *m/z*: 479.0 [M + H], HRSM Calcd. for C$_{28}$H$_{27}$N$_6$O$_2$ [M + H]$^{+}$: *m/z* = 479.2195; Found: 479.2199. Yield: 17%.

N-(2-Aminophenyl)-1-{4-[2-(1*H*-indol-3-yl)acetamido]phenyl}-5-methyl-1*H*-pyrazole-3-carboxamide (**15e**): ^{1}H NMR (400 MHz, DMSO-*d*^{6}) δ 10.90 (d, *J* = 2.5 Hz, 1H), 10.33 (s, 1H), 9.35 (s, 1H), 7.83–7.74 (m, 2H), 7.61 (d, *J* = 7.8 Hz, 1H), 7.53 (d, *J* = 8.9 Hz, 2H), 7.37–7.25 (m, 3H), 7.16–6.88 (m, 3H), 6.82–6.70 (m, 2H), 6.60 (td, *J* = 7.5, 1.5 Hz, 1H), 4.90 (s, 2H), 3.76 (s, 2H), 2.31 (s, 3H). ^{13}C NMR (101 MHz, DMSO-*d*^{6}) δ 170.49, 160.39, 146.75, 142.57, 141.30,

139.87, 136.58, 134.22, 127.67, 125.95, 125.83, 124.41, 124.18, 121.45, 119.72, 119.13, 118.87, 117.18, 117.01, 111.84, 108.81, 107.61, 34.29, 12.45. TLC: 1:1 (EtOAc/heptane). MS *m/z*: 464.9 [M + H], HRSM Calcd. for C$_{27}$H$_{25}$N$_6$O$_2$ [M + H]$^{+}$: *m/z* = 465.2039; Found: 465.2036. HPLC: rt 11.75 min (purity 97.3%). Yield: 23%.

N-(2-Aminophenyl)-5-methyl-1-{4-[2-(1-methyl-1*H*-indol-3-yl)acetamido]phenyl}-1*H*-pyrazole-3-carboxamide (**15f**): ^{1}H NMR (400 MHz, DMSO-*d*^{6}) δ 10.34 (s, 1H), 9.35 (s, 1H), 7.78 (d, *J* = 9.0 Hz, 2H), 7.62 (d, *J* = 7.8 Hz, 1H), 7.53 (d, *J* = 8.9 Hz, 2H), 7.39 (d, *J* = 8.2 Hz, 1H), 7.31 (d, *J* = 7.9 Hz, 1H), 7.25 (s, 1H), 7.16–7.10 (m, 1H), 7.02 (t, *J* = 7.5 Hz, 1H), 6.95–6.89 (m, 1H), 6.77 (d, *J* = 7.9 Hz, 1H), 6.72 (s, 1H), 6.60 (t, *J* = 7.5 Hz, 1H), 4.87 (s, 2H), 3.75 (s, 5H), 2.31 (s, 3H) ^{13}C NMR (101 MHz, DMSO-*d*^{6}) δ 170.34, 160.39, 146.75, 142.47, 141.31, 139.81, 137.00, 134.27, 128.68, 127.98, 126.35, 125.96, 125.83, 124.23, 121.60, 119.75, 119.32, 119.00, 117.26, 117.06, 110.04, 108.08, 107.62, 34.07, 32.74, 13.55, 12.45. TLC: 1:1 (EtOAc/heptane). MS *m/z*: 479.0 [M + H], HRSM Calcd. for C$_{28}$H$_{26}$N$_6$O$_2$Na [M + H]$^{+}$: *m/z* = 501.2015; Found: 501.2013. HPLC: rt 12.69 min (purity 94.3%). Yield: 65%.

N-[2-Amino-5-(thiophen-2-yl)phenyl]-1-{4-[2-(1*H*-indol-3-yl)acetamido]phenyl}-5-methyl-1*H*-pyrazole-3-carboxamide (**15h**): ^{1}H NMR (400 MHz, DMSO-*d*^{6}) δ 10.91 (s, 1H), 10.33 (s, 1H), 9.45 (s, 1H), 7.78 (d, *J* = 9.1 Hz, 2H), 7.63–7.59 (m, 2H), 7.54 (d, *J* = 9.0 Hz, 2H), 7.38–7.31 (m, 1H), 7.29–7.19 (m, 3H), 7.09–7.02 (m, 2H), 7.00–6.93 (m, 1H), 6.80 (d, *J* = 8.3 Hz, 2H), 6.74 (s, 1H), 5.06 (s, 2H), 3.76 (s, 2H), 2.32 (s, 3H). ^{13}C NMR (126 MHz, DMSO-*d*^{6}) δ 169.85, 162.08, 143.61, 142.40, 139.79, 139.63, 136.26, 134.16, 129.57, 128.79, 127.15, 127.04, 126.25, 123.68, 119.82, 116.68, 116.52, 115.80, 43.78, 11.95. TLC: 1:1 (EtOAc/heptane). MS *m/z*: 547.2 [M + H], HRSM Calcd. for C$_{32}$H$_{29}$N$_6$O$_2$S [M + H]$^{+}$: *m/z* = 561.2073; Found: 561.2073. HPLC: rt 14.19 min (purity 97.5%). Yield: 25%.

N-[2-Amino-5-(thiophen-2-yl)phenyl]-5-methyl-1-{4-[2-(1-methyl-1*H*-indol-3-yl)acetamido]phenyl}-1*H*-pyrazole-3-carboxamide (**15i**): ^{1}H NMR (400 MHz, DMSO-*d*^{6}) δ 10.34 (s, 1H), 9.45 (s, 1H), 7.78 (d, *J* = 9.0 Hz, 2H), 7.62 (d, *J* = 5.9 Hz, 2H), 7.54 (d, *J* = 8.9 Hz, 2H), 7.40 – 7.37 (m, 1H), 7.34 (d, *J* = 6.3 Hz, 1H), 7.26–7.20 (m, 3H), 7.16–7.11 (m, 1H), 7.06–6.99 (m, 2H), 6.80 (d, *J* = 8.3 Hz, 1H), 6.74 (s, 1H), 5.06 (s, 2H), 3.75 (s, 5H), 2.32 (s, 3H). ^{13}C NMR (101 MHz, DMSO-*d*^{6}) δ 170.47, 160.60, 146.63, 144.73, 142.58, 141.35, 139.85, 136.59, 134.25, 131.97, 128.64, 127.66, 125.96, 124.40, 124.19, 123.88, 123.77, 123.27, 123.12, 121.56, 121.48, 119.74, 119.10, 118.89, 117.23, 111.85, 108.79, 107.68, 34.31, 12.46. TLC: 1:1 (EtOAc/heptane). HRSM Calcd. for C$_{31}$H$_{27}$N$_6$O$_2$S [M + H]$^{+}$: *m/z* = 547.1916; Found: 547.1911. HPLC: rt 13.49 min (purity 95.7%), MS *m/z*: 561.2 [M + H]. Yield: 23%.

4.1.8 | General procedure for the synthesis of final compound 12a–e, 15a–d, and 15g

The amino compounds **11a,b** and **14a–d** (0.04 mmol) were dissolved with triethyl amine (TEA) (1.5 mmol; 0.155 g) in 30 mL of dry THF and stirred at 0°C. Acyl chloride (0.06 mmol) was added dropwise to the

previous mixture then the reaction was stirred for 3 h. The reaction was quenched with ice and extracted with EtOAc. The organic extract was washed with 1 N NaHCO$_3$, dried over anhydrous Na$_2$SO$_4$, filtered, and concentrated under reduced pressure. The obtained solid was purified by MPLC (Heptane: EtOAc) (54%). The obtained solid was dissolved in DCM (5 mL), and then TFA (5 mL) was added at 0°C. The reaction mixture was stirred at RT for 1 h. The solvent was evaporated to dryness, and 1 N NaOH (20 mL) was added to the residue and the mixture was stirred for 1 h, then it was extracted with EtOAc. The organic extract was washed with brine, dried over anhydrous Na$_2$SO$_4$, filtered, and concentrated under reduced pressure. The residue was purified by using MPLC (DCM/MeOH) (2%–4%) to provide the corresponding amide.

N-(2-Aminophenyl)-1-(4-acetamidophenyl)-5-methyl-1*H*-pyrazole-4-carboxamide (**12a**): ^{1}H NMR (400 MHz, DMSO-*d^6*) δ 10.16 (s, 1H), 9.29 (s, 1H), 8.25 (s, 1H), 7.73 (d, *J* = 8.8 Hz, 2H), 7.43 (d, *J* = 8.8 Hz, 2H), 7.12 (dd, *J* = 7.8, 1.5 Hz, 1H), 6.94 (td, *J* = 7.6, 1.6 Hz, 1H), 6.76 (dd, *J* = 8.0, 1.5 Hz, 1H), 6.58 (td, *J* = 7.5, 1.5 Hz, 1H), 4.86 (s, 2H), 2.49 (s, 3H), 2.07 (s, 3H). ^{13}C NMR (101 MHz, DMSO-*d^6*) δ 169.03, 162.09, 143.61, 142.39, 139.76, 133.95, 127.15, 126.74, 126.22, 123.69, 119.65, 116.69, 116.52, 115.78, 24.49, 11.96. TLC: 9.5:0.5(CHCl$_3$/MeOH). MS *m/z*: 347.9 [M−H]$^-$, HRSM Calcd. for C$_{19}$H$_{19}$N$_5$O$_2$Na [M+Na]$^+$: *m/z* = 372.1436; Found: 372.1430. HPLC: rt 8.98 min (purity 98.2% %). Yield: 42%.

N-[2-Amino-5-(thiophen-2-yl)phenyl]-1-(4-acetamidophenyl)-5-methyl-1*H*-pyrazole-4-carboxamide (**12b**): ^{1}H NMR (400 MHz, DMSO-*d^6*) δ 10.24 (s, 1H), 10.08 (s, 1H), 8.44 (s, 1H), 7.76 (d, *J* = 8.9 Hz, 2H), 7.72 (d, *J* = 2.2 Hz, 1H), 7.57–7.50 (m, 2H), 7.49–7.40 (m, 3H), 7.30 (d, *J* = 8.3 Hz, 1H), 7.12 (dd, *J* = 5.1, 3.6 Hz, 1H), 4.89 (s, 2H), 2.52 (s, 3H), 2.07 (s, 3H). ^{13}C NMR (101 MHz, DMSO-*d^6*) δ 169.08, 162.55, 143.07, 142.80, 140.11, 139.94, 133.75, 129.03, 126.25, 126.11, 123.94, 123.74, 119.69, 115.16, 24.50, 12.07. TLC: 9.5:0.5(CHCl$_3$/MeOH). MS *m/z*: 432.1 [M + H]$^+$, HRSM Calcd. for C$_{23}$H$_{22}$N$_5$O$_2$S [M + H]$^+$: *m/z* = 432.1494; Found: 432.1496. HPLC: rt 11.84 min (purity 99.1% %). Yield: 29%.

N-{4-Amino-2'-methoxy-[1,1'-biphenyl]-3-yl}-1-(4-acetamidophenyl)-5-methyl-1*H*-pyrazole-4-carboxamide (**12c**): ^{1}H NMR (400 MHz, DMSO-*d^6*) δ 10.34 (s, 1H), 10.28 (s, 1H), 8.55 (s, 1H), 7.76 (d, *J* = 8.9 Hz, 2H), 7.67 (d, *J* = 2.0 Hz, 1H), 7.50 (d, *J* = 8.3 Hz, 1H), 7.46–7.36 (m, 3H), 7.35 (d, *J* = 1.8 Hz, 1H), 7.30 (dd, *J* = 7.5, 1.7 Hz, 1H), 7.12 (dd, *J* = 8.4, 1.1 Hz, 1H), 7.04 (td, *J* = 7.5, 1.1 Hz, 1H), 4.88 (s, 2H), 3.77 (s, 3H), 2.52 (s, 3H), 2.07 (s, 3H). ^{13}C NMR (101 MHz, DMSO-*d^6*) δ 169.09, 162.53, 156.53, 143.21, 140.20, 139.97, 138.39, 133.71, 131.56, 130.71, 129.90, 128.74, 127.86, 127.54, 126.25, 124.02, 121.32, 119.68, 115.07, 112.35, 56.05, 24.49, 12.07. TLC: 9.5:0.5(CHCl$_3$/MeOH). MS *m/z*: 455.9 [M + H]$^+$, 453.9 [M−H]$^-$, HRSM Calcd. for C$_{26}$H$_{26}$N$_5$O$_3$ [M + H]$^+$: *m/z* = 456.2035; Found: 456.2034. HPLC: rt 11.98 min (purity 99.9%). Yield: 32%.

N-{4-Amino-3'-methoxy-[1,1'-biphenyl]-3-yl}-1-(4-acetamidophenyl)-5-methyl-1*H*-pyrazole-4-carboxamide (**12d**): ^{1}H NMR (400 MHz, DMSO-*d^6*) δ 10.24 (s, 1H), 10.16 (s, 1H), 8.47 (s, 1H), 7.76 (d, *J* = 8.3 Hz, 3H), 7.56 (d, *J* = 8.2 Hz, 1H), 7.48–7.33 (m, 3H), 7.21 (d, *J* = 7.8 Hz, 1H), 6.93 (d, *J* = 5.7 Hz, 1H), 4.87 (s, 2H), 3.81 (s, 3H), 2.52 (s, 4H), 2.07 (s, 3H). ^{13}C NMR (101 MHz, DMSO-*d^6*) δ 169.08, 162.56, 160.26, 143.07, 140.96, 140.13, 139.93, 134.03, 130.56, 129.52, 128.63, 126.25, 125.40, 125.27,

119.69, 119.21, 115.02, 113.62, 112.40, 55.64, 24.49, 12.07. TLC: 9.5:0.5(CHCl$_3$/MeOH). MS *m/z*: 456 [M + H]$^+$, HRSM Calcd. for C$_{26}$H$_{26}$N$_5$O$_3$ [M + H]$^+$: *m/z* = 456.2035; Found: 456.2030. HPLC: rt 12.30 min (purity 97.5% %). Yield: 34%.

N-(2-Aminophenyl)-5-methyl-1-[4-(2-phenylacetamido)phenyl]-1*H*-pyrazole-4-carboxamide (**12e**): ^{1}H NMR (400 MHz, DMSO-*d^6*) δ 10.39 (s, 1H), 9.29 (s, 1H), 8.25 (s, 1H), 7.76 (d, *J* = 9.0 Hz, 2H), 7.44 (d, *J* = 8.9 Hz, 2H), 7.36–7.28 (m, 4H), 7.12 (d, *J* = 7.8 Hz, 1H), 6.96–6.91 (m, 1H), 6.76 (d, *J* = 7.9 Hz, 1H), 6.62–6.52 (m, 2H), 4.85 (s, 2H), 3.67 (s, 2H), 2.3 (s, 3H). ^{13}C NMR (101 MHz, DMSO-*d^6*) δ 169.85, 143.61, 142.40, 139.79, 139.63, 136.26, 134.16, 129.57, 128.79, 127.15, 127.04, 126.74, 126.25, 123.68, 119.82, 116.68, 116.52, 115.80, 43.78, 11.95. TLC: 9.5:0.5 (CHCl$_3$/MeOH). MS *m/z*: 425.9 [M + H], HRSM Calcd. for C$_{25}$H$_{24}$N$_5$O$_2$ [M + H]$^+$: *m/z* = 426.1930; Found: 426.1931. HPLC: rt 11.38 min (purity 98.9%). Yield: 21%.

N-(2-Aminophenyl)-1-(4-acetamidophenyl)-5-methyl-1*H*-pyrazole-3-carboxamide (**15a**): ^{1}H NMR (400 MHz, DMSO-*d^6*) δ 10.30 (s, 1H), 10.07 (s, 1H), 7.84–7.74 (m, 2H), 7.59–7.48 (m, 3H), 7.39–7.32 (m, 1H), 7.25 (dd, *J* = 6.0, 3.2 Hz, 2H), 6.80 (d, *J* = 0.9 Hz, 1H), 2.32 (d, *J* = 0.8 Hz, 3H), 2.08 (s, 3H). ^{13}C NMR (101 MHz, DMSO-*d^6*) δ 206.90, 169.10, 161.07, 145.94, 141.56, 140.02, 133.99, 127.46, 126.89, 126.03, 123.97, 119.62, 107.91, 24.50, 12.43. TLC: 9.5:0.5(CHCl$_3$/MeOH). MS *m/z*: 350.2 [M + H]$^+$, 347.8 [M−H]$^-$, HRSM Calcd. for C$_{19}$H$_{20}$N$_5$O$_2$ [M + H]$^+$: *m/z* = 350.1617; Found: 350.1618. HPLC: rt 9.58 min (purity 96.2% %). Yield: 44%.

N-[2-Amino-5-(thiophen-2-yl)phenyl]-1-(4-acetamidophenyl)-5-methyl-1*H*-pyrazole-3-carboxamide (**15b**): ^{1}H NMR (400 MHz, DMSO-*d^6*) δ 10.29 (s, 1H), 10.07 (s, 1H), 7.82–7.74 (m, 3H), 7.59–7.48 (m, 4H), 7.44 (d, *J* = 2.4 Hz, 1H), 7.31 (d, *J* = 8.3 Hz, 1H), 7.12 (dd, *J* = 5.1, 3.6 Hz, 1H), 6.81 (s, 1H), 2.33 (s, 3H), 2.08 (s, 3H). ^{13}C NMR (101 MHz, DMSO-*d^6*) δ 169.10, 161.05, 146.01, 142.82, 141.57, 139.99, 134.02, 129.01, 126.14, 126.03, 124.10, 123.83, 123.77, 119.63, 107.89, 24.51, 12.44. TLC: 9.5:0.5(CHCl$_3$/MeOH). MS *m/z*: 431.9 [M + H]$^+$, HRSM Calcd. for C$_{23}$H$_{22}$N$_5$O$_2$S [M + H]$^+$: *m/z* = 432.1494; Found: 432.1492. HPLC: rt 12.42 min (purity 99.1% %). Yield: 39%.

N-(2-Amino-4-fluorophenyl)-1-(4-acetamidophenyl)-5-methyl-1*H*-pyrazole-3-carboxamide (**15c**): ^{1}H NMR (400 MHz, DMSO-*d^6*) δ 10.15 (s, 1H), 9.32 (s, 1H), 7.74 (d, *J* = 8.8 Hz, 2H), 7.58–7.48 (m, 2H), 7.18 (dd, *J* = 8.7, 6.3 Hz, 1H), 6.71 (s, 1H), 6.53 (dd, *J* = 11.2, 2.9 Hz, 1H), 6.35 (td, *J* = 8.6, 2.9 Hz, 1H), 5.13 (s, 2H), 2.31 (s, 3H), 2.07 (s, 3H). ^{13}C NMR (101 MHz, DMSO-*d^6*) δ 169.04, 160.73, 159.96, 146.63, 145.31, 145.19, 141.23, 139.77, 134.18, 128.12, 128.02, 125.99, 119.88, 119.60, 107.62, 102.91, 102.68, 102.46, 102.21, 24.50, 12.43. TLC: 9.5:0.5 (CHCl$_3$/MeOH). MS *m/z*: 367.8 [M + H], HRSM Calcd. for C$_{19}$H$_{19}$N$_5$O$_2$F [M + H]$^+$: *m/z* = 368.1522; Found: 368.1522. HPLC: rt 10.48 min (purity 95.2% %). Yield: 29%.

N-(2-Aminophenyl)-5-methyl-1-[4-(2-phenylacetamido)phenyl]-1*H*-pyrazole-3-carboxamide (**15d**): ^{1}H NMR (400 MHz, DMSO-*d^6*) δ 10.39 (s, 1H), 9.34 (s, 1H), 7.77 (d, *J* = 9.0 Hz, 2H), 7.54 (d, *J* = 8.9 Hz, 2H), 7.35–7.21 (m, 6H), 6.93 (d, *J* = 9.5 Hz, 1H), 6.77 (d, *J* = 8.0 Hz, 1H), 6.72 (s, 1H), 6.63–6.55 (m, 1H), 4.81 (s, 2H), 3.67 (d, *J* = 2.1 Hz, 2H), 2.31 (s, 3H). ^{13}C NMR (101 MHz, DMSO-*d^6*) δ 169.84, 160.37, 146.79,

142.58, 141.31, 139.63, 136.24, 134.39, 129.59, 128.79, 127.05, 125.98, 125.82, 124.18, 119.78, 117.18, 117.01, 107.64, 43.78, 12.46. MS *m/z*: 425.9 [M + H], HRSM Calcd. for $C_{25}H_{24}N_5O_2$ [M + H]⁺: *m/z* = 426.1930; Found: 426.1932. HPLC: rt 11.93 min (purity 100%). Yield: 77%.

N-[2-Amino-5-(thiophen-2-yl)phenyl]-5-methyl-1-[4-(2-phenylacetamido)phenyl]-1*H*-pyrazole-3-carboxamide (**15g**): ¹H NMR (400 MHz, DMSO-*d⁶*) δ 10.42 (s, 1H), 9.45 (s, 1H), 7.78 (d, *J* = 9.0 Hz, 2H), 7.61 (d, *J* = 2.2 Hz, 1H), 7.55 (d, *J* = 9.0 Hz, 2H), 7.37–7.30 (m, 6H), 7.28–7.20 (m, 2H), 7.05–7.00 (m, 1H), 6.80 (d, *J* = 8.4 Hz, 1H), 6.74 (s, 1H), 5.06 (s, 2H), 3.67 (s, 2H), 2.32 (s, 3H). ¹³C NMR (126 MHz, DMSO-*d⁶*) δ 169.87, 160.60, 146.66, 144.74, 142.60, 141.36, 139.67, 136.25, 134.40, 129.60, 128.80, 128.66, 127.06, 125.99, 124.19, 123.89, 123.78, 123.28, 123.13, 121.57, 119.80, 117.23, 107.72, 43.79, 12.48. TLC: 1:1 (EtOAc/heptane). HPLC: rt 13.73 min (purity 97.9%), MS *m/z*: 508.2 [M + H]. HRSM Calcd. for $C_{29}H_{26}N_5O_2S$ [M + H]⁺: *m/z* = 508.1807; Found: 508.1810. Yield: 20%.

4.2 | In vitro HDAC 1, 2, and 3 assays

The in vitro testing on recombinant HDAC 1, 2, and 3 was performed as previously described.[15] In short, recombinant human proteins HDAC1, HDAC2, and HDAC3/NCOR1 were purchased from ENZO Life Sciences AG. HDACs 1–3 were tested using a fluorogenic peptide derived from p53 (Ac-RHKK(Acetyl)-AMC. As assay buffer 50 mM 4-(2-hydroxyethyl)-1-piperazineethanesulfonic acid, 150 mM NaCl, 5 mM $MgCl_2$, 1 mM tris(2-carboxyethyl)phosphin, and 0.2 mg/mL BSA was used and the pH 7.4 was adjusted with NaOH. Inhibitor concentrations were incubated with 10 nM HDAC1, 3 nM HDAC2, or 3 nM HDAC3 (final concentration) for 5 min. The reaction was first started with the addition of the peptide substrate (20 µM final concentration) and incubated for 60 min for HDAC2 and HDAC3 at room temperature and 90 min for HDAC1 at 37°C. The reaction was then stopped with a solution of 1 mg/mL trypsin and 20 µM suberoylanilide hydroxamic acid (SAHA) in buffer and incubated for 1 h at room temperature. The fluorescence intensity was measured using an Envision 2104 Multilabel plate reader (PerkinElmer) with an excitation wavelength of 380 ± 8 nm and an emission wavelength of 430 ± 8 nm. The measured fluorescence intensities were normalized with the uninhibited reaction as 100% and the reaction without enzyme as 0%. A nonlinear regression analysis was done to determine the IC_{50} value.

4.3 | Molecular modeling

Schrödinger Suite 2019 was employed for molecular modeling studies. For visualization, Maestro was utilized.[31]

4.3.1 | Protein preparation

Protein structures were prepared using Protein Preparation Wizard.[32,33] Hydrogen atoms were added and bond orders were assigned to create zero-order bonds to metals. Water molecules 5 Å away from the ligands were deleted. Filling in missing side chains and loops using Prime[34–36] was performed. Ionization states of the ligands were generated using Epik[37–39] at pH 7.0 ± 2.0. Hydrogen bonds were optimized by sampling water orientation and utilizing PROPKA at pH 7.0. For the current study crystal structures of HDAC1 PDB: 4BKX and HDAC2 PDB: 4LY1 were used which have been evaluated in previous work.[15,25]

4.3.2 | Grid generation

The Receptor Grid Generation panel was used to generate the grids by utilizing the centroid of the ligand as the center of the grid. Since the HDAC1 crystal structure is an apo form, it was first minimized in the presence of the HDAC2 ligand after copying the ligand co-ordinates as reported before.[15,25]

4.3.3 | Ligand preparation

Ligands including the original ligands were prepared utilizing the LigPrep[40] panel with OPLS3e force fields. Possible states including metal binding states were generated at a target pH of 7 ± 2.

4.3.4 | Docking setup

Docking was performed using Glide[41–44] with flexible ligand sampling and standard precision. Five poses were subjected to post-docking minimization and reporting the top-scored pose. To validate the docking protocol, re-docking of the original ligand in HDAC2 was performed and the RMSD between the native pose and the docked pose was found to be 0.187 Å.

4.3.5 | MDs simulations

The predicted binding mode of the inhibitors was subjected to further inspection by means of MD simulation using Desmond[45,46] and utilizing OPLS2005 force fields. Each protein–ligand complex was simulated for 50 ns for two independent runs as well as a single MD run of 250 ns. The system was solvated in a simple point charge water model with an orthorhombic box and a 10 Å distance between the solute and the box boundary. The box volume was then minimized. Neutralization of the system was performed by adding chloride ions 4 Å from the ligand.

The prepared system was relaxed by employing the default Desmond relaxation protocol for the isobaric-isothermal (NPT) ensemble, then followed by a production run with the NPT ensemble at the temperature of 300 K using a Nose–Hoover chain thermostat and a pressure of 1.01325 bar using Martyna–Tobias–Klein barostat. The progress of the simulation was recorded every 100 ps.

For analysis, the Simulation Event Analysis panel was used for the RMSD of the zinc ion by fitting to the protein backbone as well as

the distance calculations between the zinc ion and the chelator atoms of the ZBG. The Simulation Interaction Diagram panel was used for analyzing the RMSD of the protein and the ligands in addition to the RMSF and the interaction persistence of the ligands.

4.4 | Cellular testing

To ascertain the EC_{50} values of compounds **12b**, **15b**, **15i**, and Entinostat in leukemia, 5×10^3 MV-4-11 cells were seeded in a 96-well plate. Subsequently, a progressive dilution series (1:4) of the compounds was executed, starting from $20\,\mu M$, and these compounds were added to the cells alongside dimethyl sulfoxide (DMSO) as a control condition. Following 72 h treatment duration, the cell viability was quantified using CellTiter-Glo® (G7572; Promega) and adjusted relative to the DMSO control. The determination of EC_{50} values was achieved through the utilization of GraphPad Prism software (version 10.1.1) employing nonlinear regression analysis.

For Western Blot analysis, 2×10^5 MV4-11 cells were seeded in a 6-well plate and incubated for 72 h at EC_{50} concentration (5 µM 12b; 200 nM Entinostat), 10 µM (**15i**), or 20 µM (**15b**), respectively, due to incomplete cell killing with **15i** and **15b**. Harvested cells were lysed in total lysis buffer (50 mM Tris (pH 7.4), 50 mM NaCl, 1% SDS (v/v), 2 mM $MgCl_2$) supplemented with 0.5 µl Benzonase® (Merck Millipore) per 100 µL. Protein concentrations were determined using the *DC Protein Assay* (Bio-Rad), according to the manufacturer's instructions, and the GloMAX Discover (Promega) at 600 nm. A BSA standard curve (0–10 mg/mL) served as a quantification control. For SDS-PAGE, 4x NuPAGE LDS Sample Buffer (Invitrogen) supplemented with 100 mM dithiothreitol was added to the protein lysates and incubated for 3 min at 95°C. Separation of proteins was accomplished on a NuPAGE Novex 4%–12% Bis-Tris protein gel (Invitrogen) with MOPS SDS-running buffer (50 mM MOPS, 50 mM Tris, 0.1% SDS (v/v), 1 mM EDTA). The SeeBlue Plus2 Pre-Stained Protein Standard (Thermo Fisher) served as a marker for size detection. Subsequently, proteins were transferred using NuPAGE transfer buffer (50 mM Tris, 40 mM glycerol, 0.04% SDS [v/v], 10% methanol [v/v]) by wet blotting onto a nitrocellulose membrane (GE Healthcare). Finally, membranes were blocked with 5% (w/v) milk. Protein expression was analyzed by Western blot analysis with primary antibodies by using fluorescence-coupled secondary antibodies and an infrared scanner (Li-Cor). The following antibodies were used: Histone H3 acetylation (06-599, Merck Millipore) and Histone H3 (14269S, Cell Signaling).

CONFLICTS OF INTEREST STATEMENT
The authors declare no conflicts of interest.

ORCID
Fady Baselious https://orcid.org/0000-0003-3242-8514
Sebastian Hilscher https://orcid.org/0009-0003-0611-7365
Stefan Hüttelmaier https://orcid.org/0000-0001-9335-4227
Mike Schutkowski https://orcid.org/0000-0003-0919-7076
Wolfgang Sippl https://orcid.org/0000-0002-5985-9261
Hany S. Ibrahim https://orcid.org/0000-0002-1048-4059

REFERENCES
[1] G. Millán-Zambrano, A. Burton, A. J. Bannister, R. Schneider, *Nat. Rev. Genet.* **2022**, *23*(9), 563.
[2] M. J. Ramaiah, A. D. Tangutur, R. R. Manyam, *Life Sci.* **2021**, *277*, 119504.
[3] G. Li, Y. Tian, W.-G. Zhu, *Front. Cell. Dev. Biol.* **2020**, *8*, 576946.
[4] S.-Y. Park, J.-S. Kim, *Exp. Mol. Med.* **2020**, *52*(2), 204.
[5] E. Seto, M. Yoshida., *Cold Spring Harbor Perspect. Biol.* **2014**, *6*(4), a018713.
[6] B. Cheng, W. Pan, Y. Xiao, Z. Ding, Y. Zhou, X. Fei, J. Liu, Z. Su, X. Peng, J. Chen, *Eur. J. Med. Chem.* **2024**, *265*, 116129.
[7] N. C. Payne, R. Mazitschek, *Cell Chem. Biol.* **2022**, *29*(7), 1140.
[8] O. Witt, H. E. Deubzer, T. Milde, I. Oehme, *Cancer Lett.* **2009**, *277*(1), 8.
[9] A. D. Bondarev, M. M. Attwood, J. Jonsson, V. N. Chubarev, V. V. Tarasov, H. B. Schiöth, *Br. J. Clin. Pharmacol.* **2021**, *87*(12), 4577.
[10] S. Shen, A. P. Kozikowski, *ChemMedChem* **2016**, *11*(1), 15.
[11] L. Ny, H. Jespersen, J. Karlsson, S. Alsén, S. Filges, C. All-Eriksson, B. Andersson, A. Carneiro, H. Helgadottir, M. Levin, I. Ljuslinder, R. Olofsson Bagge, V. R. Sah, U. Stierner, A. Ståhlberg, G. Ullenhag, L. M. Nilsson, J. A. Nilsson, *Nat. Commun.* **2021**, *12*(1), 5155.
[12] M. L. Johnson, R. Gonzalez, M. Opyrchal, D. Gabrilovich, P. Ordentlich, S. Brouwer, S. Sankoh, E. V. Schmidt, M. L. Meyers, S. S. Agarwala, *J. Clin. Oncol.* **2017**, *35*(15_suppl), 9529.
[13] N. Masuda, K. Tamura, H. Yasojima, A. Shimomura, M. Sawaki, M.-J. Lee, A. Yuno, J. Trepel, R. Kimura, Y. Nishimura, S. Saji, H. Iwata, *BMC Cancer* **2021**, *21*(1), 1269.
[14] M. L. Johnson, J. Strauss, M. R. Patel, E. B. Garon, K. D. Eaton, T. Neskorik, J. Morin, R. Chao, B. Halmos., *Clin. Lung Cancer* **2023**, *24*(3), 218.
[15] H. S. Ibrahim, M. Abdelsalam, Y. Zeyn, M. Zessin, A.-H. M. Mustafa, M. A. Fischer, P. Zeyen, P. Sun, E. F. Bülbül, A. Vecchio, F. Erdmann, M. Schmidt, D. Robaa, C. Barinka, C. Romier, M. Schutkowski, O. H. Krämer, W. Sippl., *Int. J. Mol. Sci.* **2022**, *23*(1), 369.
[16] M. Abdelsalam, M. Zmyslia, K. Schmidtkunz, A. Vecchio, S. Hilscher, H. S. Ibrahim, M. Schutkowski, M. Jung, C. Jessen-Trefzer, W. Sippl, *Arch. Pharm.* **2024**, *357*(n/a), e2300536.
[17] J. Zhang, X. Gao, L. Yu., *Front. Oncol.* **2021**, *11*, 741746.
[18] E. Vagapova, M. Kozlov, T. Lebedev, K. Ivanenko, O. Leonova, V. Popenko, P. Spirin, S. Kochetkov, V. Prassolov, *Biomedicines* **2021**, *9*(12), 1846.
[19] O. M. Moradei, T. C. Mallais, S. Frechette, I. Paquin, P. E. Tessier, S. M. Leit, M. Fournel, C. Bonfils, M.-C. Trachy-Bourget, J. Liu, T. P. Yan, A.-H. Lu, J. Rahil, J. Wang, S. Lefebvre, Z. Li, A. F. Vaisburg, J. M. Besterman, *J. Med. Chem.* **2007**, *50*(23), 5543.
[20] F. F. Wagner, M. Weïwer, S. Steinbacher, A. Schomburg, P. Reinemer, J. P. Gale, A. J. Campbell, S. L. Fisher, W.-N. Zhao, S. A. Reis, K. M. Hennig, M. Thomas, P. Müller, M. R. Jefson,

D. M. Fass, S. J. Haggarty, Y.-L. Zhang, E. B. Holson, *Bioorg. Med. Chem.* **2016**, *24*(18), 4008.

[21] I. Hubeek, E. M. Comijn, C. L. Van Der Wilt, R. L. Merriman, J. M. Padron, G. J. Kaspers, G. J. Peters, *Oncol. Rep.* **2008**, *19*(6), 1517.

[22] L. K. Gediya, A. Belosay, A. Khandelwal, P. Purushottamachar, V. C. Njar, *Bioorg. Med. Chem.* **2008**, *16*(6), 3352.

[23] M. Loprevite, M. Tiseo, F. Grossi, T. Scolaro, C. Semino, A. Pandolfi, R. Favoni, A. Ardizzoni *Oncol. Res.* **2005**, *15*(1), 39.

[24] V. Marquardt, J. Theruvath, D. Pauck, D. Picard, N. Qin, L. Blümel, M. Maue, J. Bartl, U. Ahmadov, M. Langini, F.-D. Meyer, A. Cole, J. Cruz-Cruz, C. M. Graef, M. Wölfl, T. Milde, O. Witt, A. Erdreich-Epstein, G. Leprivier, U. Kahlert, A. Stefanski, K. Stühler, S. T. Keir, D. D. Bigner, J. Hauer, T. Beez, C. B. Knobbe-Thomsen, U. Fischer, J. Felsberg, F. K. Hansen, R. Vibhakar, S. Venkatraman, S. H. Cheshier, G. Reifenberger, A. Borkhardt, T. Kurz, M. Remke, S. Mitra, *J. Immunother. Cancer* **2023**, *11*(1), e005871.

[25] E. F. Bülbül, J. Melesina, H. S. Ibrahim, M. Abdelsalam, A. Vecchio, D. Robaa, M. Zessin, M. Schutkowski, W. Sippl, *Molecules* **2022**, *27*(8), 2526.

[26] H. S. Ibrahim, S. M. Abou-Seri, M. Tanc, M. M. Elaasser, H. A. Abdel-Aziz, C. T. Supuran, *Eur. J. Med. Chem.* **2015**, *103*, 583.

[27] J. Liu, Y. Yu, J. Kelly, D. Sha, A.-B. Alhassan, W. Yu, M. M. Maletic, J. L. Duffy, D. J. Klein, M. K. Holloway, S. Carroll, B. J. Howell, R. J. O. Barnard, S. Wolkenberg, J. A. Kozlowski, *ACS Med. Chem. Lett.* **2020**, *11*(12), 2476.

[28] L. Whitehead, M. R. Dobler, B. Radetich, Y. Zhu, P. W. Atadja, T. Claiborne, J. E. Grob, A. Mcriner, M. R. Pancost, A. Patnaik, W. Shao, M. Shultz, R. Tichkule, R. A. Tommasi, B. Vash, P. Wang, T. Stams, *Bioorg. Med. Chem.* **2011**, *19*(15), 4626.

[29] F. Baselious, D. Robaa, W. Sippl, *Comput. Biol. Med.* **2023**, *167*, 107700.

[30] C. Boldron, A. Besse, M.-F. Bordes, S. Tissandié, X. Yvon, B. Gau, A. Badorc, T. Rousseaux, G. Barré, J. Meneyrol, G. Zech, M. Nazare, V. Fossey, A.-M. Pflieger, S. Bonnet-Lignon, L. Millet, C. Briot, F. Dol, J.-P. Hérault, P. Savi, G. Lassalle, N. Delesque, J.-M. Herbert, F. Bono, *J. Med. Chem.* **2014**, *57*(17), 7293.

[31] Schrödinger Release 2019-1: Maestro, Schrödinger, LLC, New York, NY, **2019**.

[32] G. Madhavi Sastry, M. Adzhigirey, T. Day, R. Annabhimoju, W. Sherman, *J. Comput.-Aided Mol. Des.* **2013**, *27*(3), 221.

[33] Schrödinger Release 2019-1: Protein Preparation Wizard; Epik, Schrödinger, LLC, New York, NY, 2019; Impact, Schrödinger, LLC, New York, NY, 2019; Prime, Schrödinger, LLC, New York, NY, **2019**.

[34] M. P. Jacobson, D. L. Pincus, C. S. Rapp, T. J. F. Day, B. Honig, D. E. Shaw, R. A. Friesner, *Proteins: Struct. Funct. Bioinf.* **2004**, *55*(2), 35

[35] M. P. Jacobson, R. A. Friesner, Z. Xiang, B. Honig, *J. Mol. Biol.* **2002**, *320*(3), 597.

[36] Schrödinger Release 2019-1: Prime, Schrödinger, LLC, New York, NY, **2019**.

[37] J. R. Greenwood, D. Calkins, A. P. Sullivan, J. C. Shelley, *J. Comput.-Aided Mol. Des.* **2010**, *24*(6–7), 591.

[38] J. C. Shelley, A. Cholleti, L. L. Frye, J. R. Greenwood, M. R. Timlin, M. Uchimaya, *J. Comput.-Aided Mol. Des.* **2007**, *21*(12), 681.

[39] Schrödinger Release 2019-1: Epik, Schrödinger, LLC, New York, NY, **2019**.

[40] Schrödinger Release 2019-1: LigPrep, Schrödinger, LLC, New York, NY, **2019**.

[41] R. A. Friesner, R. B. Murphy, M. P. Repasky, L. L. Frye, J. R. Greenwood, T. A. Halgren, P. C. Sanschagrin, D. T. Mainz, *J. Med. Chem.* **2006**, *49*(21), 6177.

[42] R. A. Friesner, J. L. Banks, R. B. Murphy, T. A. Halgren, J. J. Klicic, D. T. Mainz, M. P. Repasky, E. H. Knoll, M. Shelley, J. K. Perry, D. E. Shaw, P. Francis, P. S. Shenkin, *J. Med. Chem.* **2004**, *47*(7), 1739.

[43] T. A. Halgren, R. B. Murphy, R. A. Friesner, H. S. Beard, L. L. Frye, W. T. Pollard, J. L. Banks, *J. Med. Chem.* **2004**, *47*(7), 1750.

[44] Schrödinger Release 2019-1: Glide, Schrödinger, LLC, New York, NY, **2019**.

[45] K. J. Bowers, D. E. Chow, H. Xu, R. O. Dror, M. P. Eastwood, B. A. Gregersen, J. L. Klepeis, I. Kolossvary, M. A. Moraes, F. D. Sacerdoti, J. K. Salmon, Y. Shan, D. E. Shaw. Scalable Algorithms for Molecular Dynamics Simulations on Commodity Clusters. In *SC '06: Proceedings of the 2006 ACM/IEEE Conference on Supercomputing*, 11-17 Nov. 2006, 2006; pp 43. https://doi.org/10.1109/SC.2006.54

[46] Schrödinger Release 2019-1; Desmond Molecular Dynamics System, D.E. Shaw Research: New York, NY, USA, 2019; Maestro-Desmond Interoperability Tools, Schrödinger: New York, NY, USA, **2019**.

SUPPORTING INFORMATION

Additional supporting information can be found online in the Supporting Information section at the end of this article.